Lattice Weyl-Wigner formulation of exact many-body quantum-transport theory and applications to novel solid-state quantum-based devices

F. A. Buot and K. L. Jensen
Naval Research Laboratory, Washington, D.C. 20375
(Received 21 September 1989; revised manuscript received 17 August 1990)

The use of the lattice-space Weyl-Wigner formalism of the quantum dynamics of particles in solids, coupled with nonequilibrium Green's-function techniques, provides a rigorous and straightforward derivation of an exact integral form of the equation for a quantum distribution function in many-body quantum-transport theory. We show that with the present formalism more realistic calculations, both numerical (particularly, highly transient simulations) and analytical (fully gauge-invariant calculations), which include full quantum effects and many-body effects, can be carried out in a straightforward, elegant, and physically meaningful manner. This is demonstrated by new results based on a more-accurate numerical simulation procedure and novel applications in terms of "quantum particle trajectories" for resonant tunneling diodes, and by a straightforward and fully gauge-invariant formulation of the exact quantum-transport equation of a uniform electron-phonon scattering system in high electric fields, which, for the first time, do not involve any gradient expansion.

I. INTRODUCTION

Discussions of quantum transport in the literature, starting with the work of Kadanoff and Baym[1] and Keldysh,[2] using Green's-function techniques for irreversible systems initiated by Schwinger,[3] often focused on the derivation of the so-called quantum Boltzmann equation (QBE).[4-7] The accuracy of the formalisms and final results given are often confined to the accuracy of the original formalism given by Kadanoff and Baym[1] several years ago, which has been discussed recently in more detail by Mahan[7] in the light of the current revival of interest in high-field quantum transport. These results are given in terms of first-order gradient expansion from the very beginning, based on the assumption of slowly varying quantities in space and time, and therefore preclude full quantum effects of tunneling and interference, effects that dominate quantum-based heterostructure-device characteristics such as in resonant tunneling diodes[8-11] (RTD's) and Aharanov-Bohm–effect devices. Moreover, gradient expansion theories often lead to rather complicated and cumbersome equations containing higher-order derivatives. In heterojunction quantum-based devices, strong nonuniformity in space coupled with very-high-frequency operation[8-10] almost always invalidates these assumptions.

The work reported here is in part motivated by the complete lack in the literature of a many-body quantum-transport formulation of irreversible systems to all orders in the gradients which is needed to give theoretical support to the advances of quantum-based device analysis and numerical simulation. As we shall show shortly, the inclusion of all orders in the gradients is surprisingly straightforward and renders the resulting expressions in rather simple and compact integral forms, more suitable for numerical work than the equations of the gradient expansion theories. With a view on applications to realistic multidimensional device structures, the coupling of quantum-transport numerical techniques with self-consistent ensemble-particle Monte Carlo techniques will further enhance the applicability of basic transport physics for modeling all regions of novel heterojunction devices. A way to accurately couple ensemble particle Monte Carlo with space- and time-dependent quantum tunneling has recently been advocated by the authors[12] via a transformation of quantum transport into a "quantum-particle-trajectory" representation.[10] Thus, we have to transform the quantum-transport solution into a particle-trajectory representation, in terms of Wigner trajectories, describing the elementary space- and time-dependent events in quantum-transport processes.

The purpose of this paper is to give an exact formulation of the many-body quantum-transport theory in phase space, to avoid the cumbersome gradient expansion procedure of previous theories, and to show, by using some very technological important examples, that real calculations on "active" or highly nonlinear solid-state quantum-based devices can conveniently be done in the quantum-distribution-function approach. It should be emphasized at the outset that the kind of problems we are considering are those found in very high-speed (highly transient) and highly nonuniform active finite open systems, which generally renders other approaches based on the use of wave functions less effective, i.e., (1) one needs to use a large number of basis states to account for very short temporal and spatial scales, (2) one must also be able to describe the violent mixing of the basis states in response to the abrupt change in the input voltage, and (3) the application of the boundary condition for active open systems is rather very cumbersome for both wave-function and density-matrix techniques. Thus, a "statistical" distribution-function approach to be described here

is required.

The derivation of an exact equation for a quantum distribution function makes use of (a) the Weyl-Wigner formulation of the quantum dynamics of electrons in a solid, proposed by one of the authors (F.A.B.) several years ago,[13,14] and (b) the method of nonequilibrium Green's-function techniques[1-3] for irreversible systems. The point of this paper is that an exact quantum-transport equation can be cast in a very simple and "universal" form that, coupled with the subsidiary device boundary conditions, can be numerically implemented and demonstrated for characterizing real devices or active open systems. The validity of this approach is further discussed at the end of the paper. So far, no other quantum-transport approach can claim the same degree of success, particularly in simulating the high-speed response of the active device to a "sudden change" in bias. In fact, what has often been treated in quantum-transport theory of submicron devices is the generalized QBE for very high constant electric field. Following the formalism used in this paper, we have also treated this problem and have given a straightforward and simple derivation of an exact and fully gauge-invariant quantum-transport equation in external high electric fields.

II. EXACT FORMULATION OF SOLID-STATE MANY-BODY QUANTUM TRANSPORT THEORY IN PHASE SPACE

In the nonequilibrium Green's-function formalism (Appendix A), the time evolution of a "double-time" correlation function $G^<$, which is related to the particle density, is coupled to the retarded Green's function G^r, describing the propagation of particles. The time evolution of $G^<$ may be written as

$$\left[\frac{\partial}{\partial t_1}+\frac{\partial}{\partial t_2}\right]G^<_{\alpha\beta}(1,2)=\frac{1}{i\hbar}[\mathcal{H},G^<]_{\alpha\beta}(1,2)+\frac{1}{i\hbar}[\Sigma^<,\mathrm{Re}G^r]_{\alpha\beta}(1,2)+\frac{1}{2\hbar}\{\Sigma^<,A\}_{\alpha\beta}(1,2)-\frac{1}{2\hbar}\{\Gamma,G^<\}_{\alpha\beta}(1,2)\ , \quad (1)$$

where (1,2) stands for $(\mathbf{q}_1,t_1,\mathbf{q}_2,t_2)$. The quantities entering in Eq. (1) are defined in the Wannier representation as follows:

$$\mathcal{H}_{\alpha\beta}(1,2)=\left[E_\alpha\left[-\frac{\hbar}{i}\nabla_1\right]+V(1)\right]\delta_{\alpha\beta}\delta(1-2)+\delta(t_1-t_2)\Sigma^{\mathrm{HF}}_{\alpha\beta}(\mathbf{q}_1,\mathbf{q}_2,t_1)+\mathrm{Re}\Sigma^r_{\alpha\beta}(1,2)\ , \quad (2)$$

$$\mathrm{Re}G^r_{\alpha\beta}(1,2)=\frac{-i}{2}\epsilon(t_1-t_2)A_{\alpha\beta}(1,2)\ , \quad (3)$$

$$\mathrm{Re}\Sigma^r_{\alpha\beta}(1,2)=\frac{-i}{2}\epsilon(t_1-t_2)\Gamma_{\alpha\beta}(1,2)\ , \quad (4)$$

$$A_{\alpha\beta}(1,2)=-2\,\mathrm{Im}G^r_{\alpha\beta}(1,2)=i[G^>_{\alpha\beta}(1,2)-G^<_{\alpha\beta}(1,2)]\ , \quad (5)$$

$$\Gamma_{\alpha\beta}(1,2)=-2\,\mathrm{Im}\Sigma^r_{\alpha\beta}(1,2)=i[\Sigma^>_{\alpha\beta}(1,2)-\Sigma^<_{\alpha\beta}(1,2)]\ , \quad (6)$$

$$\epsilon(t_1-t_2)=\Theta(t_1-t_2)-\Theta(t_2-t_1)\ . \quad (7)$$

In Eqs. (1) and (2), $V(1)$ is the matrix element, between two Wannier functions, of a spin-independent external potential. $E_\alpha(k)$ is the exact Bloch electron energy-band function, and Σ^{HF} is the Hartree-Fock approximation to the self-energy; square brackets indicate commutation of operators separated by a comma, curly brackets indicate anticommutation of operators separated by a comma, and the greek indices label band indices, including spin. The equation for G^r obeys the Dyson equation and is given by

$$G^r_{\alpha\beta}=G^{0r}_{\alpha\beta}+G^{0r}_{\alpha\sigma}\Sigma^r_{\sigma\eta}G^r_{\eta\beta}\ . \quad (8)$$

For simplicity in what follows we will consider only a one-band model, which often holds in semiconductor transport, and drop the greek indices altogether. However, the inclusion of multiband indices is straightforward and the treatment is analogous to the method given by Korenman[15] in his work on gas lasers. We will also treat the lattice point coordinates occurring in all of the above equations, written in the Wannier representation, as approximated by a continuum for simplicity of presentation. The reader is referred to the previous work[13,14] of one of the authors (F.A.B.) for rigorous formulation of the lattice-space Weyl-Wigner formulation of band electron dynamics.

We transform the space-time variables as follows:

$$t_1=T-\tau/2,\quad \mathbf{q}_1=\mathbf{q}-\mathbf{v}/2\ ,\qquad t_2=T+\tau/2,\quad q_2=\mathbf{q}+\mathbf{v}/2\ , \quad (9)$$

and define a (3+1)-dimensional "momentum" vector p and its conjugate variable q as

$$p=(\mathbf{p},E),\quad E=\hbar\omega\ ,\qquad q=(\mathbf{q},T)\ , \quad (10)$$

which allows us to also write $v=(\mathbf{v},\tau)$. In terms of the new variables we write the arguments in Eq. (1) by replacing (1,2) by $(\mathbf{v},\tau,\mathbf{q},T)$. The Weyl transform, $a(p,q)$, of any operator $\hat{A}$ is defined by the following relation:[13,14]

$$a(p,q)=\int dv\, e^{(i/\hbar)p\cdot v}\langle q-\tfrac{1}{2}v|\hat{A}|q+\tfrac{1}{2}v\rangle\equiv\mathcal{W}A(\mathbf{v},\tau,\mathbf{q},T)\ , \quad (11)$$

where the matrix element in the integrand is evaluated between two Wannier functions. Therefore, if we take the Weyl transform of both sides of Eq. (1) we will immediately obtain a phase-space–frequency-time domain evolution equation for $G^<(p,q)$. In most works on quantum transport, starting with the work of Kadanoff and Baym,[1] the "transformation to center-of-mass coordinates," often employed to derive the gradient expansion,

effectively define the corresponding Weyl transform with the energy variable E in Eq. (11) replaced by $-E$. Therefore, in comparing our results with those obtained by others, we may have to replace E by $-E$ and $\partial/\partial E$ by $-\partial/\partial E$.

To evaluate the Weyl transform of terms involving commutator and anticommutator on the right-hand side (RHS) of Eq. (1), we use the following relations, which are valid for any operator $\hat{A}$ and $\hat{B}$:

$$\mathcal{W}[\hat{A},\hat{B}](\mathbf{v},\tau,\mathbf{q},T)=2i\sin(\hat{\Lambda})a(p,q)b(p,q)\ , \tag{12}$$

$$\mathcal{W}\{\hat{A},\hat{B}\}(\mathbf{v},\tau,\mathbf{q}T)=2\cos(\hat{\Lambda})a(p,q)b(p,q)\ , \tag{13}$$

where

$$\hat{\Lambda}=\frac{\hbar}{2}\left[\frac{\partial^{(a)}}{\partial q}\cdot\frac{\partial^{(b)}}{\partial p}-\frac{\partial^{(a)}}{\partial p}\cdot\frac{\partial^{(b)}}{\partial q}\right]$$

is the "Poisson-bracket" differential operator. Therefore Eq. (1), in the phase-space–energy-time domain, becomes

$$\frac{\partial}{\partial T}G^{<}(\mathbf{p},E,\mathbf{q},T)=\frac{2}{\hbar}\sin(\hat{\Lambda})[H(p,q)G^{<}(p,q)+\Sigma^{<}(p,q)\mathrm{Re}G^{r}(p,q)]+\frac{1}{\hbar}\cos(\hat{\Lambda})[\Sigma^{<}(p,q)A(p,q)-\Gamma(p,q)G^{<}(p,q)]\ . \tag{14}$$

Using the definition of Weyl transform, Eq. (11), and making use of the "exponential" displacement operation, we may also write the RHS of Eq. (14) in an integral operator form as

$$\begin{aligned}\frac{\partial}{\partial t}(-i)G^{<}(\mathbf{p},E,\mathbf{q},t)=&\frac{2}{(h^4)^2}\int dp'dq'K_H^s(p,q-q';q,p-p')(-i)G^{<}(p',q')\\&+\frac{2}{(h^4)^2}\int dp'dq'K_{\Sigma<}^s(p,q-q';q,p-p')(-i)\mathrm{Re}G^{r}(p',q')\\&-\frac{2}{(h^4)^2}\int dp'dq'K_{\Sigma<}^c(p,q-q';q,p-p')(-i)\mathrm{Im}G^{r}(p'q')\\&-\frac{1}{(h^4)^2}\int dp'dq'K_{\Gamma}^c(p,q-q';q,p-p')(-i)G^{<}(p',q')\ ,\end{aligned} \tag{15}$$

where $(-i)G^{<}(\mathbf{p},E,\mathbf{q},t)$ is a real-valued quantum distribution function. The integral kernels which have very simple forms are derived in Appendix B. These are given in terms of the Weyl transform of the operator, indicated in the subscript of the kernel, as follows:

$$K_a^s(p,q-q';q,p-p')=\int dv\,dj\exp\left[\frac{2i}{\hbar}j\cdot(q-q')\right]\left[a\left[p-j,q+\frac{v}{2}\right]-a\left[p+j,q-\frac{v}{2}\right]\right]\sin\left[\frac{(p-p')\cdot v}{\hbar}\right]\ , \tag{16}$$

$$K_a^c(p,q-q';q,p-p')=\int dv\,dj\exp\left[\frac{2i}{\hbar}j\cdot(q-q')\right]\left[a\left[p-j,q+\frac{v}{2}\right]+a\left[p+j,q-\frac{v}{2}\right]\right]\cos\left[\frac{(p-p')\cdot v}{\hbar}\right]\ . \tag{17}$$

The exact time-evolution equation for the Wigner distribution function $f_w(\mathbf{p},\mathbf{q},t)$ immediately follows from Eq. (15) by integrating with respect to energy E, using the relation

$$f_w(\mathbf{p},\mathbf{q},t)=\frac{1}{h}\int dE(-i)G^{<}(\mathbf{p},E,\mathbf{q},t)\ . \tag{18}$$

Equation (15) describes all types of transport phenomena without any assumption as to strength of the variation of all quantities, the sort of assumptions common to all previous studies of many-body quantum-transport theory. Though very important in quantum-based device physics, to the authors' knowledge, Eqs. (14) and (15) are not found in the literature. The first two terms in the RHS of Eqs. (14) and (15), which arise from a commutation of two operators in Eq. (1), may be viewed as describing the generalized quantized motion of particles in phase space with a more complicated energy-momentum relation due to the influence of potential and scatterings. The last two terms in these equations, which arise from the anticommutation of two operators in Eq. (1), describe particle transfers in phase space due to collisions and scatterings and correspond to the collision terms in the classical Boltzmann equation. In other words, whereas the first two terms of Eqs. (14) and (15) account for the complicated quantization of particle motions (i.e., includes quantum tunneling and interference phenomena) in phase space, the last two terms account for the "broadening effects" on these motions due to scatterings and collisions. Indeed, for slowly varying systems, and for conditions of the validity of QBE to hold, the contributions coming from the second term of Eqs. (14) and (15) can also be neglected leading to the relaxation type of approximation to the collision terms in the QBE.

It is important to emphasize at this point that we have effectively cast the notoriously complicated and rather very cumbersome many-body quantum-transport theory based on gradient expansion (bad for numerical work) in a very compact and simple integral form (good for numerical work) in which one can hope to be able to do real calculations for characterizing highly nonlinear devices. The essential attribute of Eqs. (14) and (15) is that they avoid, surprisingly for the first time, any gradient expan-

sion and therefore incorporate the full quantum effects needed to simulate resonant-tunneling and quantum-interference (Aharanov-Bohm effect) devices. In Sec. III, we will demonstrate this type of calculation in the device characterization of resonant-tunneling diodes by considering the subsidiary device-boundary conditions pertinent to these devices. The success of this approach in simulating highly transient situations is mainly due to the compatibility of the quantum-distribution-function approach to the boundary conditions existing in active quantum-based semiconductor devices, and to the numerical stability inherent in the simple form of the integro-differential equation, Eq. (15). The approach, based on the use of subsidiary device boundary condition, also bears exact correspondence in the limit $\hbar \to 0$ to the proven classical approach on finite active open systems described by the Boltzmann equation.

III. REAL CALCULATIONS OF THE FULL QUANTUM EFFECTS IN RESONANT-TUNNELING DIODES

Although the nonequilibrium Green's-function technique of many-body quantum transport has conceptually formulated the quantum-transport problem, difficulties arise when one does actual calculations, either numerical or analytical. What has happened is that formulation of quantum transport bent on doing actual calculations always proceeded from the very beginning as a gradient expansion, often up to first order in the gradient, to be manageable, based on the assumption of slowly varying quantities.[4-7] These assumptions are clearly invalid for real quantum-based and highly nonlinear devices. What we have done in Sec. II is to put the nonequilibrium Green's-function technique in a new "dress," specifically put it in the framework of the lattice Weyl-Wigner formulation of the quantum dynamics of band electrons in solids, so as to avoid gradient expansion altogether. In this section, we will demonstrate that with the present formalism highly transient calculations of semiconductor active devices can be done, in the sense that one can simulate the current response of the device with respect to a sudden switch in the voltage bias. Approaches based on the use of wave functions or a finite number of basis states are not suitable for simulating this highly transient behavior of active devices, since one has to account for the "violent mixing" of a large number of basis states, i.e., the current response generally contains a wide band of Fourier components in the frequency domain.

Since the virtue of the present formalism, which sets it apart from other approaches, is that it avoids the gradient expansion, we will retain this important attribute in performing the device characterization of a RTD. To simplify the present numerical demonstration, we neglect the broadening effects to the electron motion caused by the collisions and therefore neglect the last two terms of Eq. (21). We also neglect the second-order kinetic correction to the particle motion coming from the second term of Eq. (15). Consistent with these approximations, we approximate the momentum-energy relation of the electrons with the effective-mass approximation; this approximation absorbs any consistent contribution from Σ^{HF} and $\mathrm{Re}\Sigma^{r}$ to $H(\mathbf{p},\mathbf{q})$.

$H(p,q)$ in Eq. (15) can be written in the effective-mass approximation as

$$H(p,q)=\frac{\mathbf{p}^2}{2m^*}+V(\mathbf{q}) , \tag{19}$$

where $V(q)$ may be taken to be the nonuniform energy band-edge profile of a RTD. The real-valued quantum-distribution-function equation, in the absence of collisions and scatterings, then reduces to the following expression:

$$\frac{\partial}{\partial t}(-i)G^{<}(\mathbf{p},E,\mathbf{q},t)=-\frac{p}{m^*}\nabla_{\mathbf{q}}(-i)G^{<}(\mathbf{p},E,\mathbf{q},t) + \frac{1}{h^4}\int d\mathbf{p}'d\mathbf{v}\left[V\left[\mathbf{q}+\frac{\mathbf{v}}{2}\right]-V\left[\mathbf{q}-\frac{\mathbf{v}}{2}\right]\right]\sin\left[\left[\frac{\mathbf{p}-\mathbf{p}'}{\hbar}\right]\cdot\mathbf{v}\right](-i)G^{<}(\mathbf{p}',E,\mathbf{q},t) . \tag{20}$$

After integrating with respect to E, the Wigner distribution-function equation follows:

$$\frac{\partial}{\partial t}f_w(\mathbf{p},\mathbf{q},t)=-\frac{p}{m^*}\nabla_{\mathbf{q}}f_w(\mathbf{p},\mathbf{q},t)+\frac{1}{h^4}\int d\mathbf{p}'d\mathbf{v}\left[V\left[\mathbf{q}+\frac{\mathbf{v}}{2}\right]-V\left[\mathbf{q}-\frac{\mathbf{v}}{2}\right]\right]\sin\left[\left[\frac{\mathbf{p}-\mathbf{p}'}{\hbar}\right]\cdot\mathbf{v}\right]f_w(\mathbf{p}',\mathbf{q},t) . \tag{21}$$

One observes that in terms of numerical implementation, the above simplified transport equations are not different from the exact equation since both have the same mathematical form of the integrals involved. However, the exact equation involves a higher-multidimensional integral than the last two equations. It is therefore reasonable to expect that given enough computational resources, one might be able to make advances in applying the exact equation, Eq. (15), to real devices. The last equation is of the form of the time-evolution equation for the Wigner distribution function for noninteracting particles. A random-phase approximation to the electron-electron interactions within the mean-field approximation can easily be incorporated in the numerical simulation of active devices by simultaneously solving the Poisson equation together with Eqs. (15), (20), or (21); however, this is not critical to the present demonstration although we have obtained in Sec. VII some results which show the effect of including self-consistency of the potential with respect to the charge distribution.

We have applied the last equation to the device characterization of resonant-tunneling diodes, which may be

thought of as a double-barrier heterojunction configuration, composed of, for example, a higher band-gap $Al_{1-x}Ga_xAs$ layer, which sandwiches a "quantum well," composed of a GaAs layer. It should be pointed out that this is not the first time that the Wigner distribution function has been used to study tunneling devices.[8] However, the numerical methods used and the method of applications are unique in our approach as will be described below. The numerical model and method of application (in terms of "Wigner trajectories") we use enables us to determine the discrete resonant energy levels, the current-voltage (I-V) characteristics, switching times, and tunneling times[10] across the device. The distribution-function approach to quantum transport owes part of its success to its ability to simulate "natural" boundary conditions of active devices, allowing for the introduction of current flow and irreversibility, i.e., it is able to simulate open systems in a manner analogous to the treatment based on the classical Boltzmann equation. "Natural" boundary conditions are taken to mean that, far from the quantum influence of the double-barrier region in RTD's, the distribution of electrons entering the device is known (e.g., equilibrium Fermi-Dirac distribution, integrated over the perpendicular momentum directions for electrons coming from a zero-field "metallic" contact region or a highly screened, heavily doped region of the device by virtue of the Markovian hypothesis for these regions[8]), and the distribution of electrons exiting is unknown and depends on the manner in which the device functions. The assumed boundary condition has been self-consistently verified in the calculations to determine its accuracy. This is determined from the solution in the neighborhood of the assumed boundary. For an accurate assumed boundary condition, the obtained solution (for a sufficiently large computational box size) must join smoothly or must be equal to the assumed values at the boundaries for the incoming particles. The authors were indeed the first to investigate the self-consistency aspects (and its dependence on the computational box size) of the boundary condition, described in detail in Ref. 16. Below, we give a brief explanation of how the Wigner distribution function is numerically calculated for a device simulation in order to show some of the unique aspects of our more exact numerical procedure and applications to RTD as compared to others.[8,11]

Evaluating $f_w(\mathbf{q},\mathbf{p},t)$ for the one-dimensional RTD involves integrating out the transverse components of $\mathbf{q}$ and $\mathbf{p}$ to obtain $f(x,k;t)$, where $x=q_x$ and $hk=p_x$, and defining $f(x,k)$ on the points of a lattice, i.e., $f(x(i),k(j))=f(i,j)$, where

$$x(i)=(i-1)L/(N_x-1)=(i-1)\epsilon ,$$

and

$$k(j)=(2j-N_k-1)\pi/\epsilon N_k=(2j-N_k-1)\delta/2 .$$

The expression for $k(j)$ is dictated by the requirements of the discrete Fourier transform. The discrete version of the RHS of Eq. (21) becomes

$$\begin{aligned}\partial_t f(i,j)&=h^{-1}\mathcal{L}\cdot f(i,j)\\&=-[hk(j)\delta/m^*]\Delta_i f(i,j)\\&\quad-\sum_{j'}V(i,j-j')f(i,j') ,\end{aligned}$$

$$V(i,j-j')=(2/N_k)\sum_{i'}\sin[(2\pi/N_k)(i'-1)(j-j')]\times[V(i+i')-V(i-i')] ,$$

where Δ_i refers to the finite-differencing operator. We have used second-order finite-differencing schemes. In the case of a zero-voltage bias for the RTD's, the central difference scheme (CDS) may be used, as the calculation is then a boundary-value problem. At nonzero bias, even a steady-state calculation of Eq. (21) becomes strictly an initial value problem in real space, and a "marching" scheme must be used. Previous applications of Eq. (21) to RTD made use of the upwind-downwind differencing scheme (UDS), which is accurate to order $O(\epsilon)$ and is defined by

$$\partial_x f(x,k)\approx\pm[f(i\pm1,j)-f(i,j)]/\epsilon ,$$

where the $\pm$ refers to the upwind-downwind directions. In our calculations, we have made use of a more accurate second-order differencing scheme (SDS), in which the space derivative at the "advanced point" is approximated by using a second-order interpolating polynomial for the local space dependence of the Wigner function; it is accurate to $O(\epsilon^2)$ and is defined by

$$\partial_x f(x,k)\approx\pm[3f(i,j)-4f(i\pm1,j)+f(i\pm2,j)]/2\epsilon .$$

At zero bias, the SDS approach gives results which are much closer to a CDS calculation, where the assumed boundary condition is verified to be more highly accurate and totally self-consistent than the UDS approach.

To solve the above equation by computer, it must first be recast in terms of a matrix equation. For concreteness, let us first consider the steady-state case. To that end, define a column vector $\mathbf{f}$ such that its $[(i-1)N_k+j)]$-th component is given by $f(i,j)$. In this language, the differencing operator and the summation with $V(i,j-j')$ over (j') represent the action of a matrix $\mathcal{L}$ on the vector $\mathbf{f}$. The block-diagonal elements of this matrix are composed of the $V(i,j-j')$ terms, the parts of the differencing operator corresponding to the $f(i,j)$ terms, and the off-diagonal blocks are associated with the parts of the differencing operator corresponding to $f(i\pm1,j)$ and $f(i\pm2,j)$ terms. The matrix version of the steady-state equation then becomes $\mathcal{L}\cdot\mathbf{f}=\mathbf{b}$, where $\mathbf{b}$ contains the boundary terms. The size of the matrix $\mathcal{L}$, when in the band storage mode, is given by $(4N_k+1)N_kN_x$. Given the current computer limitations (Cray X-MP/24), the largest value of N_k and N_x that we may use are 72 and 86, respectively. In practice, solving for one steady-state distribution takes on the order of 13 CPU seconds for the UDS method and 48 CPU seconds for the SDS.

In numerically implementing the time evolution in Eq. (21), we have used for the first time an implicit and "norm-preserving" incremental time-evolution operator

in all transient simulation. If Eq. (21) is written as $i\hbar(\partial/\partial t)X_{\rm LHS}(t)=X_{\rm RHS}(t)$, then the time-evolution equation can be determined by solving at each time step the following equation [similar remarks hold for Eq. (15)]:

$$i\hbar[X_{\rm LHS}(t+\delta t)-X_{\rm LHS}(t)]/\delta t = \theta X_{\rm RHS}(t+\delta t)+(1-\theta)X_{\rm RHS}(t) \quad (0\le\theta\le 1) .$$

In applying to Eq. (21) and using $\theta=\frac{1}{2}$, this reduces to

$$(1+ir\mathcal{L})f(\mathbf{p},\mathbf{q},t+\delta t)=(1-ir\mathcal{L})f(\mathbf{p},\mathbf{q},t)$$

where $r=\delta t/2\hbar$, which leads for the Cayley form of the time-evolution operator. Putting $r=1$ set the time step of the simulation to be $\delta t=1.32\times10^{-15}$ s.

Particle density and current density may also be extracted from the Wigner function. The former, which involves a straightforward discretization of $(2\pi)^{-1}\int dk\, f(x,k)$, is simply equal to

$$n(i)=(\delta/2\pi)\sum_j f(i,j) .$$

For current densities, however, caution must be used in discretizing

$$j(x)=(2\pi)^{-1}\int (hk/m^*)f(x,k)dk .$$

We first note that in steady state, $\partial_x j(x)=0$. What we desire, then, is an expression for the current such that the operation of the finite-differencing operator on the result is identically zero. As a next step, consider the sum over j of the equation for $\mathcal{L}\cdot\mathbf{f}$. A little inspection shows that the resulting equation is proportional to the time derivative of the density in discrete form [recall that $\sum_{jj'}V(i,j-j')f(i,j')$ is already identically zero by virtue of the definition of $V(i,j)$]. But, since $\partial_t n(x)-\partial_x j(x)=0$, we may now identify

$$j(i+\tfrac{1}{2})-j(i-\tfrac{1}{2})\approx(h\delta\epsilon/2\pi m^*)\sum_j k(j)\Delta_i f(i,j) .$$

Consider, for concreteness, the expression for $\Delta_i f(i,j)$ which, after a little manipulation, may be written as

$$[3f(i,j)-f(i+1,j)]-[3f(i+1,j)-f(i+2,j)] .$$

Consequently, we see that the form of the current for the SDS approach, which results in a vanishing current gradient for steady state, may be written as

$$j(i+\tfrac{1}{2})=\frac{\hbar 4\delta\epsilon}{4\pi m^*}\left[\sum_{j=1}^{N_k/2}k(j)[3f(i+1,j)-f(i+2,j)]+\sum_{j=N_k/2+1}^{N_k}k(j)[-f(i-1,j)+3f(i,j)]\right] .$$

The expression for current in the UDS approach has been given previously.[8]

The SDS, coupled with the Cayley form of the incremental time-evolution operator, results in a more accurate approach in simulating RTD's over the simpler UDS approach. The details of the numerical aspects, such as accuracy, computer time used, and sensitivity to numerical parameters of the two approaches has been discussed in detail by Jensen and Buot in a separate paper.[16]

Unless otherwise specified, the parameters used in all of the resulting simulations are as follows. The box, barrier, and well sizes are 550, 30, and 50 Å, respectively; a density in the boundaries of 2.0×10^{18} cm^{-3}; potential barrier heights of 0.3 eV; an effective mass, constant throughout the device, of $0.0667m_0$; and a transient time step of 1.0 fs ($r=0.76$). N_x and N_k are taken to be 86 and 72, respectively. An "injected hot electron"[16] bias, which represents an accumulation of electrons in the first barrier edge and depletion after the last barrier edge, was applied across the double-barrier structure, i.e., the bias potential is given by $V_b(x)+V_0(x-x_2)/(x_1-x_2)$, where $V_b(x)$ is the RTD's band-edge profile, x_2 is 30 Å past the second barrier edge, and x_1 is 30 Å in front of the first barrier edge (in general, we have taken x_2-x_1 to equal $4L_b+L_w$) and $V_b(x)$ vanishes beyond these points. For the transient calculations, the bias was switched between the voltages corresponding to the current maximum and minimum. Unless otherwise indicated, calculations were done at 77 K. For the self-consistent potential calculations of Sec. VII, the doping density of 2.0×10^{18} cm^{-3} extends from the source and drain of the RTD's to 30 Å before the barrier edges.

Figure 1 shows the calculated I-V characteristics of a GaAs-$Al_{1-x}Ga_xAs$-GaAs-$Al_{1-x}Ga_xAs$ semiconductor heterojunction RTD, showing resonance by a single discrete level in the quantum well, as calculated by both the SDS and UDS. As is apparent from the figure, the SDS is better able to model the Wigner function near resonance. The current peak-to-valley ratio predicted by the SDS is 14.1, as compared to the UDS value of 1.37. Decreasing the barrier width and increasing the well width results in a quantum well with two discrete levels. Figure 2 shows the I-V curve for such a structure where the barriers are 20 Å and the well is 70 Å, in which the two discrete resonances are plainly visible in our simulation.

The emergence of the additional resonant energy level is expected since the number of discrete energy levels within the quantum well increases with the square root of the product of quantum well width and barrier height. Since the barrier height is kept constant in our simulation, we also expect the spacing of the first two energy levels to decrease as the well width increases. These quantum-transport results are consistent with our calculations on the transmission probability as a function of energy and voltage bias for these simulated structures.

A critical test to the accuracy of the SDS over the UDS is to compare the symmetry of the Wigner distribution functions obtained by the two different methods for a RTD at zero bias. We have also employed a novel analytical and numerical technique for characterizing the quantum-tunneling process across the double-barrier

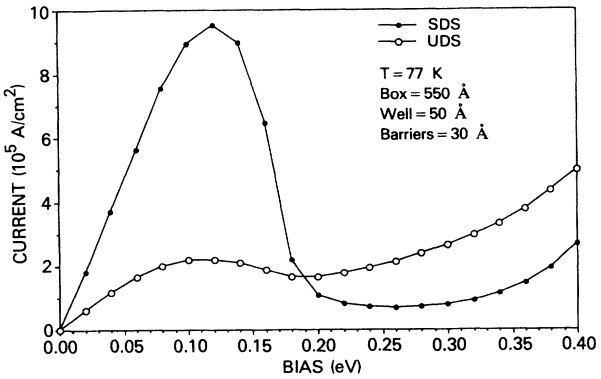

FIG. 1. Comparison of the I-V characteristics in the absence of scattering as obtained by the SDS and UDS methods. The UDS approach yields a less resolved resonant region than the more accurate SDS approach. The quantum well width is 50 Å, barrier widths are 30 Å, and barrier height is 0.3 eV.

structures by means of Wigner trajectories, described in more detail in Ref. 10, and Bohm trajectories.[17] These trajectories are quantum analog of the particle trajectories in classical mechanics and their numerical calculations have been described elsewhere.[10,12] The calculation of the Wigner trajectories depends critically on the accuracy of the Wigner distribution function calculated. The superior accuracy of the SDS over the UDS in calculating Wigner trajectories justifies the additional computer time incurred in the use of the SDS. Indeed, sample runs using a larger computational box, a larger number of mesh and improved accuracy of the descritization mesh, and using the large memory capabilities of the CRAY2 computer show marked improvement in the Wigner function and calculated trajectories.

Figure 3(a) shows a highly symmetric Wigner distribution function calculated using the CDS, which is practically identical to that obtained using the SDS, for RTD at zero bias. In contrast, the use of the UDS has yielded a significantly asymmetrical and hence incorrect Wigner

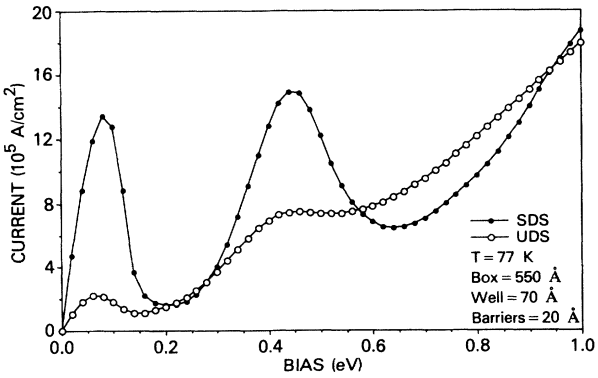

FIG. 2. The I-V characteristics resulting from the presence of two closely spaced resonant energy levels of a RTD with 20-Å barrier widths and a 70-Å quantum well width, with the same barrier height as in Fig. 1. Figures 1 and 2 also agree with our numerical calculations of the tunneling coefficients as a function of the voltage bias.

distribution function at zero bias; this asymmetry shows up very clearly in the calculated Wigner trajectories.

A number of interesting features can be seen from the resulting Wigner trajectory diagram in Fig. 3(b), which was calculated from the Wigner function distribution of Fig. 3(a). First, low-momentum states are reflected well before the barrier edge which is clearly an indication of nonlocal quantum effects. Second, trajectories which are able to tunnel through the structure seem to have been accelerated before the barrier edge, decelerated across the barriers, and accelerated within the quantum well and after traversing the second barrier. We define open or tunneling trajectories, which are accelerated within the quantum well, as nonresonant trajectories. These trajectories essentially "see" the two barriers sequentially. As we shall see in what follows, resonant-tunneling trajectories spend more time within the quantum well, and see the double-barrier structure as a "whole."

Bound trajectories, symmetrical about $k=0.0$, exist within the quantum well as expected. However, "closed-looplike" trajectories also exist, symmetrically placed above and below the $k=0.0$ axis and occur near the position where the tunneling trajectories get accelerated before crossing the barrier. These closed-looplike trajectories appear to correspond to complementary trajectories, i.e., portions of the $k>0.0$ loop are paired with portions of the $k<0.0$ loop, implying that at these regions in space the Wigner trajectories instantaneously change direction, as though the "particles" were bouncing between impenetrable potential barriers. Thus, each trajectory calculated seems to see a different "effective potential." The effective potential seen by the particle is the sum of the classical potential defined by the double-barrier configuration of the RTD's plus a nonlocal "quantum potential." Indeed, the concept of quantum potential and "Bohm trajectory" was first introduced by Bohm to explain causality in quantum mechanics.[17] The results on our trajectory analysis seem to suggest that tunneling trajectories see an attractive accelerating potential center before reaching the barrier edge of the RTD, which helps in decreasing the effectiveness of the classical barrier and consequently allows the particle to tunnel through. This conjecture is also supported by our calculation on a traveling Schrödinger wave packet, where the wave packet incident on a square barrier changes the effective potential as seen by the particles. The tunneling particles in the traveling wave-packet calculations essentially "surf-ride" the wave function, in phase with the changing effective potential across the barrier.[17]

One of the still controversial aspects of quantum theory is the concept of a quantum-tunneling time, which is really a causal and particle trajectory concept. So far, most, if not all, calculations made arbitrary use of a traveling Schrödinger wave packet to calculate tunneling times. Figure 3(c) is a plot of position versus time for open or tunneling Wigner trajectories of Fig. 3(b). The time taken for the tunneling trajectory associated with the lowest wave vector is approximately 110 fs. Note that in contrast with other calculations based on the arbitrary use of a Schrödinger traveling wave packet to calcu-

late tunneling times, our calculations are unique in that they are based on "microscopically" examining the elementary and individual space-time events in a quantum-tunneling process using the causal Wigner trajectory description.[10]

In Fig. 4 a new behavior is exhibited by some tunneling trajectories when a nonzero-voltage bias is applied to the RTD. We show only in Fig. 4(b) these tunneling trajectories which are not accelerated inside the quantum well, in contrast to those of Fig. 3(b). These trajectories spend more time in the quantum well than the nonresonant trajectories and do not appear to see the two barriers separately, but do see the RTD as a whole. These trajectories, whose initial momentum states were always found to be at or near the resonant energy level of the quantum well, will be referred to here as "resonant trajectories."

It is interesting to compare the Wigner distribution function obtained by the UDS and SDS methods for a RTD biased at the resonance region where quantum effects are dominant. The presence of stronger quantum fluctuations in the Wigner distribution function is clearly evident using the SDS method [Fig. 5(a)] compared to that obtained using the UDS method [Fig. 5(b)]. Figure 5(c) shows the calculated Wigner distribution function, obtained from Figs. 5(a) and 5(b), evaluated at the drain end of RTD's. The result using the SDS method shows more clearly a "tunneling ridge" in the Wigner distribution than the result of the UDS method. Figure 5(d) shows how the tunneling-ridge distribution at the drain end of the RTD's shifts to higher energies as the voltage bias is increased to 0.5 eV. Indeed, the tunneling ridge leads to the particlelike energetics behavior of the calcu-

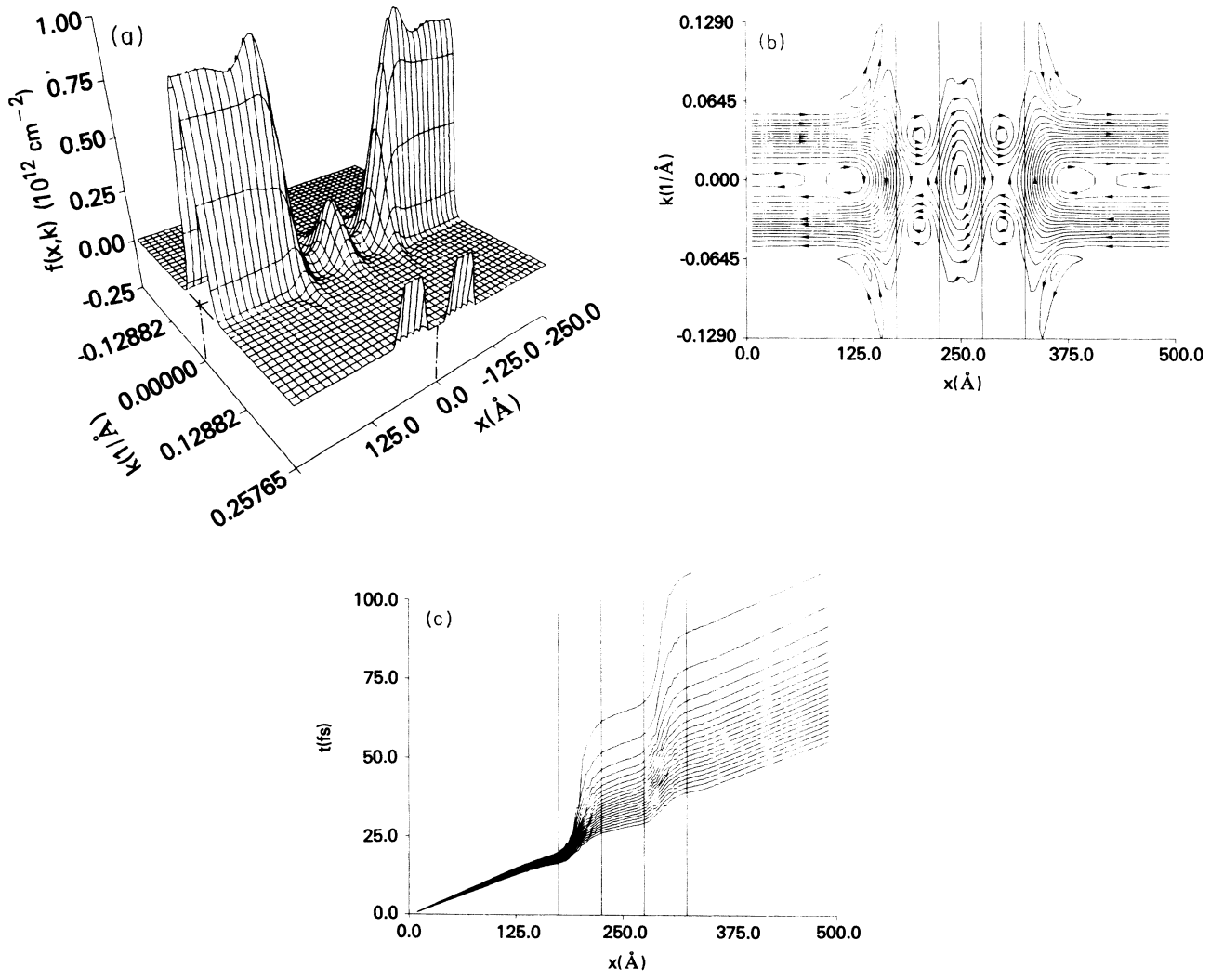

FIG. 3. (a) Wigner distribution function for a RTD with identical barrier and quantum well widths of 50 Å, at $T=300$ K, obtained by using the CDS for the space derivative. The RTD at zero bias is treated as a boundary-value problem. (b) Wigner trajectories associated with the Wigner distribution function shown in (a). The vertical lines define the location of the square potential barrier edges. Complementary "closed-looplike" trajectories located at $k>0$ and $k<0$ are discussed in the text. (c) The tunneling Wigner trajectories of (b) plotted in space-time. The velocity at any point is given by the inverse slope at that point. The trajectories define the individual and elementary space-time–dependent events in a quantum-tunneling process.

lated Wigner trajectories.[10]

The transient response of the RTD to sudden change in the voltage bias, from resonant current-peak bias to current-valley bias, is also markedly different for the UDS versus the SDS. Figure 6(a) obtained using the UDS predicts a shorter switching-time duration compared to Fig. 6(b), which is obtained using the SDS. The SDS method more accurately models the quantum fluctuations and particle densities within the quantum well than the UDS method; it is these quantum fluctuations and larger particle densities in the SDS approach and the need to satisfy the current continuity equation [Figs. 6(c)–6(e)] which lead to a switching time that is four times that of the UDS method. Many-body effects on the device characterization of the RTD discussed above will be treated in Sec. VII. There it will be shown that the effect of scattering is to reduce the device switching time, which is a marked departure from results one expects from conventional classical-device transport analysis. The effect of self-consistency in the charge and potential is also discussed there.

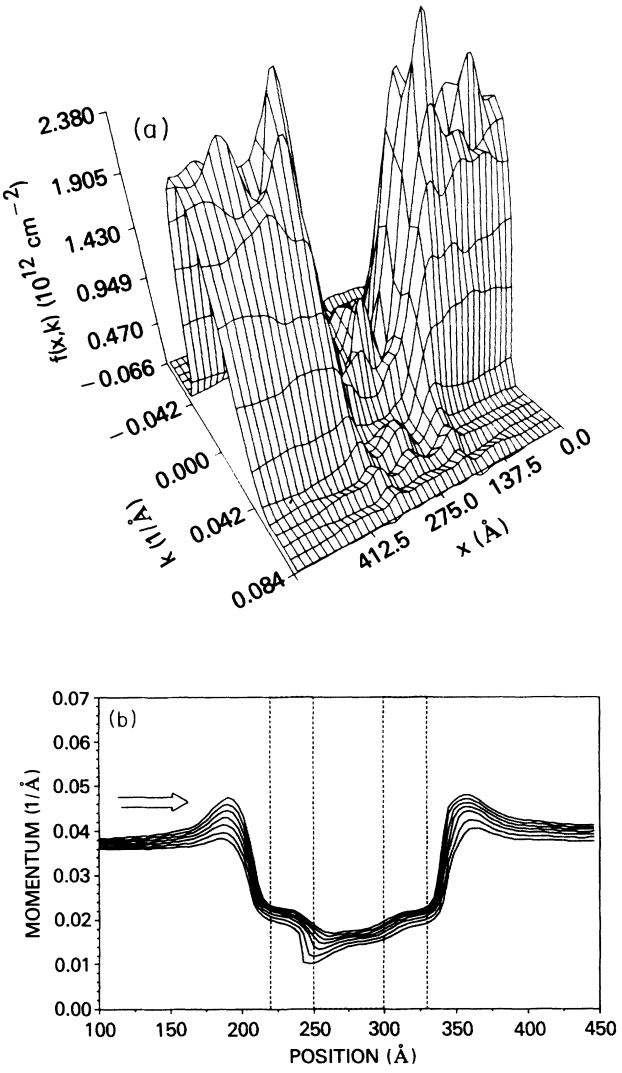

FIG. 4. (a) Wigner distribution function solution for the RTD at a small bias of 0.02 eV. The resulting tunneling Wigner trajectory pattern drastically changes from that of Fig. 3(b), as shown in (b). (b) A new behavior of the tunneling trajectories emerges when a small bias of 0.02 eV is applied to the RTD. Observe the tunneling trajectories, with initial momentum at the source around 0.039 $Å^{-1}$ corresponding to the resonant peak energy, which are not accelerated and/or decelerated within the quantum well, in contrast with the tunneling trajectories of Fig. 3(b). These are referred to as the "resonant trajectories," implying that the "particle" stays longer in the potential well. This is also supported by our numerical simulation of a traveling wave packet with a group velocity at resonance impinging the RTD.

It is important to point out that the numerical results presented here could not have been obtained using the previous many-body quantum-transport formulations which are based on gradient expansions. Clearly all QBE results are markedly different from the results obtained by Eq. (21) in the limit of vanishing self-energies and hence preclude at the outset quantum effects due to tunneling and quantum interference, and hence are not of any use for numerical simulation of RTD's. A more convincing way to show this is to examine the effective potential as seen by the particles in Eq. (21) compared with that of the QBE. Whereas in the QBE the particle essentially "feels" the classical potential, with many-body corrections from the self-energies, the particle in Eq. (21) sees an effective potential V_{eff} which is the sum of a classical potential and quantum potential, defined by the following equation:[10]

$$(\nabla_q \nabla_{\text{eff}}) \nabla_p f_w(\mathbf{p},\mathbf{q}) = \frac{1}{h} \int d\mathbf{p}' V(\mathbf{q},\mathbf{p}-\mathbf{p}') f_w(\mathbf{p}',\mathbf{q}) , \quad (22)$$

where $V(\mathbf{q},\mathbf{p})$ is defined by Eq. (21) and may include all many-body corrections just as in the QBE. V_{eff} is responsible for the tunneling mechanism in RTD's.[10] Equation (21) is accurate to all orders in the gradient expansion.

IV. EVALUATION OF THE SELF-ENERGIES

An important first step in considering many-body effects in the exact quantum-transport equation is to define the self-energies involved. A diagrammatic evaluation of the nonequilibrium Green's function defined on a contour is analogous to its equilibrium counterpart[18,19] and therefore leads us to consider the corresponding fundamental quantities of many-body theory[20] in terms of "effective interaction" and self-energies,[19] evaluated in a manner analogous to that of equilibrium many-body theory.

The first-order and lowest-order "irreducible" diagrams for the self-energy are often referred to as the Hartree-Fock approximation. For electron-impurity scattering in impure systems this corresponds to the virtual-crystal approximation. These first-order diagrams will result only in the renormalization of the energy-momentum relation for the particle. The next-order self-energy diagrams for electron-electron interactions are called the Born diagrams, and look similar to the Born approximation for the lowest-order self-energy for the electron-phonon interactions.

Higher levels of approximation for the self-energies involve infinite resummation with a selected class of irreducible diagrams to all orders in the perturbation. Most often this approach leads to the well-known Dyson equation for the quantity being sought. The self-energy is expressed in terms of effective interaction or vertex function which is approximated by a summation to all orders of bubble diagrams or "ladder" diagrams, as in the random-phase approximation (RPA) or t-matrix approximation of the vertex function. The RPA diagrams correspond to the use of dressed or effective interaction in the Born approximation.[21]

A. Self-energy for scattering by impurities

For electron scattering by impurities the single-site t-matrix method involves an infinite resummation of all terms involving repeated scattering by the same impurity site or repeated multiple scattering by the same impurity. This results in a self-energy expression which can be given either linearly in the impurity concentration for a low-concentration limit or include all orders of the concentration for a large concentration of defects, which reduces to the virtual-crystal approximation in the limit where the relative concentration of defects approaches

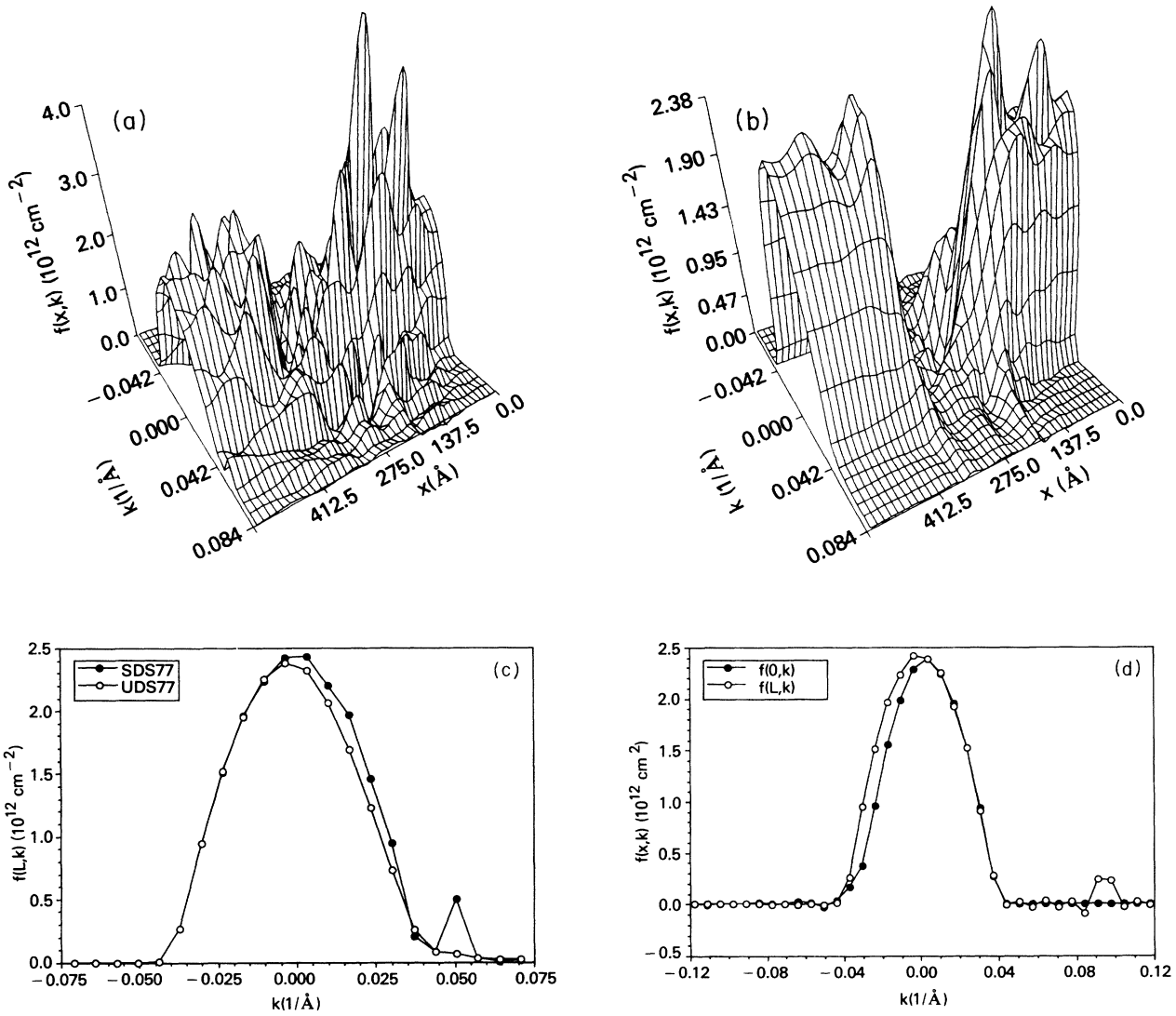

FIG. 5. (a) Wigner distribution function solution for the RTD corresponding to (b), obtained by using the SDS. Notice the presence of stronger quantum fluctuations as compared to that of (b). (b) Wigner distribution function solution for the RTD biased at resonance, $V_0=0.116$ eV, using the UDS method. This is to be compared with (a). (c) Quantum-distribution-function solution of (a) and (b), plotted at the drain end of the RTD. The tunneling-ridge distribution is more visible using the SDS approach compared to that obtained using the UDS approach. The tunneling ridge leads to conservation-of-energy behavior for the Wigner trajectories. (d) Quantum distribution function obtained by the SDS method plotted at both the source and drain end of the RTD, with a much higher voltage bias ($V_0=0.5$ eV). Notice the shift of the tunneling-ridge distribution to the higher energies. Also notice that the quantum distribution at the source end is approximately a "thermal distribution"; it is partially depleted at the higher-energy portion of the distribution for the exiting particles, since the source end represents the uphill potential for the electrons entering at the drain.

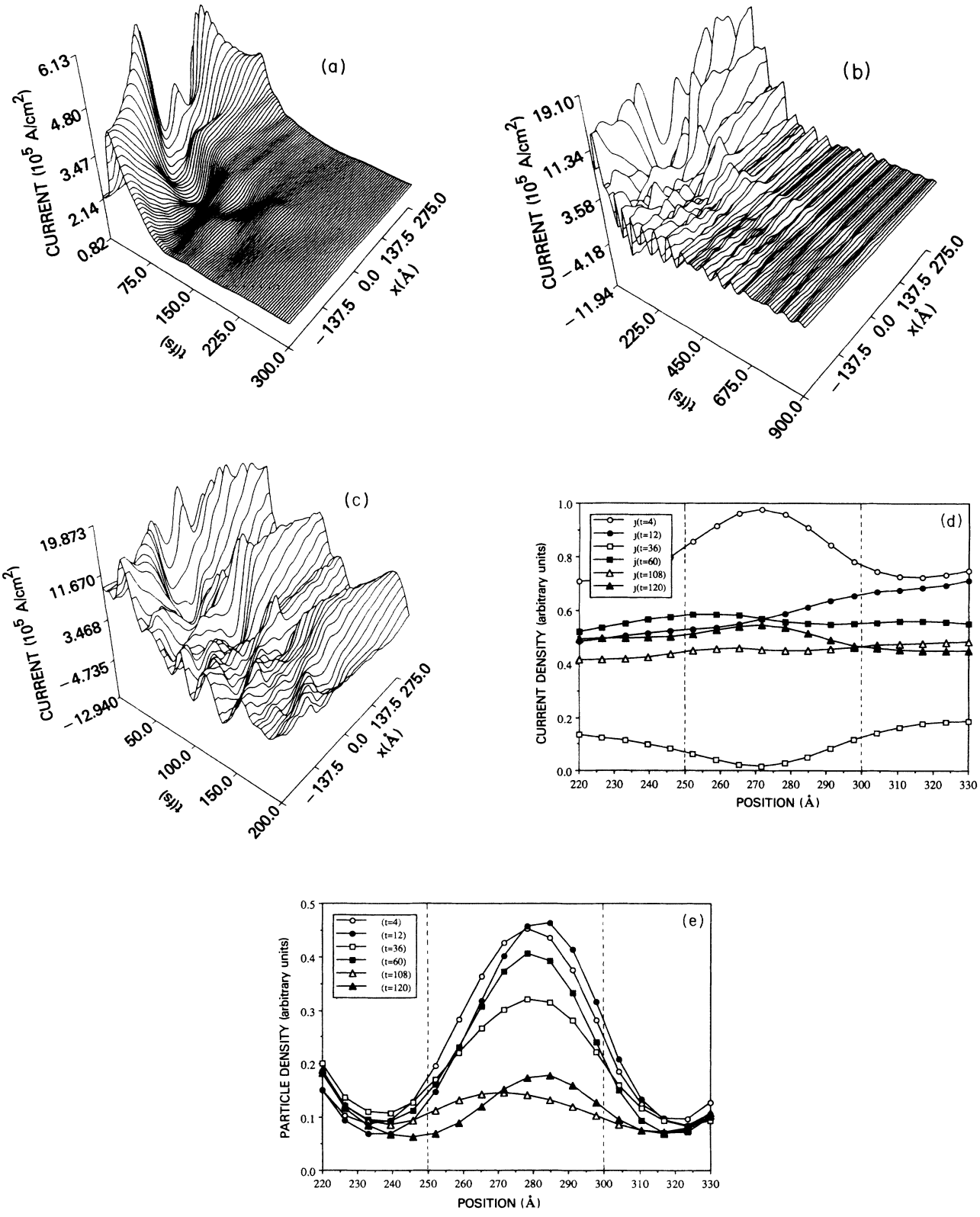

FIG. 6. (a) Transient response to a sudden switch in the voltage bias (from resonant peak to valley) of the current-density distribution within the RTD using the UDS method. (b) Transient response of the RTD in (a) using the more accurate SDS approach, which yields a much longer switching time than indicated in (a), due to "quantum ringing." (c) Details of the quantum oscillations of the current-density distribution in (b), shortly after the sudden switch of the voltage bias, showing some "quantum-ringing" of the current-density values between the source and drain of the RTD. (d) Details of the current-density distribution of (c) at the center of the RTD at different time slices. This figure is to be compared with (e), which is related through the particle conservation equation. (e) Details of the particle density distribution at the center of RTD at different time slices, corresponding to (d).

one.[22] More accurate approximation schemes for the self-energy of electron impurity scattering are referred to as the coherent-potential approximation (CPA) and are basically obtained by summing the same single-site diagrams as before but using an "effective-medium" Green's function, instead of the unperturbed Green's function of the host lattice, with a self-consistent scattering potential.[22]

For quantum-based devices made of "decent" (low concentration of defects) semiconductor materials, an approximation to the self-energy can make use of the single-site t-matrix approach for the retarded self-energy. In order to apply to the transport equation previously derived in Sec. III, we need to use Weyl-transform quantities. Confining to pure Coulombic interaction with the defects (i.e., exclude spin-dependent interactions and/or the "Kondo effect"), the Weyl transform of the retarded[20] self-energy can be written as

$$\Sigma^r(p,q)=n_i T(p,q) , \tag{23}$$

where n_i is the impurity density, and $T(p,q)$ is the Weyl transform of the T-matrix operator which can be a very complicated function of the single-site t matrix. Note that in general, the multiple single-site scattering approach will result in the expression for the self-energies which have a linear dependence with the impurity density n_i. The Weyl transform of the T matrix obeys the following equation:

$$T(p,q)=V(p,q)+\frac{1}{(h^4)^2}\int dv\,dv'\,dj\,dj'\,e^{(i/\hbar)j\cdot v'}e^{-(i/\hbar)j'\cdot v}V\left[p+j,q-\frac{v}{2}\right]T\left[p+j',q+\frac{v'}{2}\right] . \tag{24}$$

where $V(p,q)$ is the Weyl transform of the impurity potential. From the identity relations (in four-dimensional vector notation)

$$\frac{1}{h^4}\int dq e^{(-i/\hbar)(k-k^1)\cdot q}a(p,q)=a_{kk'}\delta\left[p-\left[\frac{k+k'}{2}\right]\right] , \tag{25}$$

$$a(p,q)=\int d(k-k')e^{(i/\hbar)(k-k')\cdot q}a_{kk'}\delta\left[p-\left[\frac{k+k'}{2}\right]\right] , \tag{26}$$

one can readily show that by performing the transformation of Eq. (25) to Eq. (24) one indeed gets

$$\begin{aligned}\frac{1}{h^4}\int dq\, e^{-(i/\hbar)(k-k')\cdot q}T(p,q)&\\ =\frac{1}{(h^4)^3}\int dq\,dv\,dv'\,dj\,dj'\,e^{-(i/\hbar)j'\cdot v'}e^{-(i/\hbar)j'\cdot v}e^{-(i/\hbar)(k-k')\cdot q}V\left[p+j,q-\frac{v}{2}\right]T\left[p+j',q+\frac{v'}{2}\right]&\\ +\frac{1}{h^4}\int dq e^{-(i/\hbar)(k-k')\cdot q}V(p,q) .&\end{aligned} \tag{27}$$

which reduces to the equation (in four-dimensional vector notation) in "momentum" space

$$T_{kk'}=V_{kk'}+\int d\eta\, V_{k\eta}T_{\eta k'} . \tag{28}$$

The above equation can easily be shown to be identical to the integral equation for the T matrix given by Mahan.[7]

So far we have only obtained "retarded quantities" by analogy with the equilibrium scattering theory. However, for impurity scattering problems, the equation for the self-energy defined on the contour is mathematically similar to that of the Green's-function equation defined on the contour, Eq. (A12). Therefore, using the same procedure for converting the equation defined on the contour to an equation defined in real time discussed in Appendix A, we arrived at an equation similar to Eq. (A18) for the self-energy, instead of the Green's function. Equating the matrix element for $\Sigma^<$ we also obtain an equation similar to Eq. (A20), without the second term, since $\Sigma_0^<$ is zero for impurity scattering. We have

$$\Sigma^<=\Sigma^r G^<\Sigma^a , \tag{29}$$

which can be written in terms of Weyl-transform quantities as

$$\begin{aligned}\Sigma^<(p,q)=\frac{1}{(h^4)^4}\int d\eta\,d\eta'\,d\beta\,d\beta'\,d\nu\,dv'\,dj\,dj'\,e^{-(1/\hbar)\beta\cdot\eta'}e^{-(i/\hbar)\beta'\eta}e^{-(i/\hbar)j\cdot v'}e^{-(i/\hbar)j'\cdot v}&\\ \times\Sigma^r\left[p+\beta+j,q-\frac{\eta}{2}-\frac{\nu}{2}\right]G^<\left[p+\beta+j',q-\frac{\eta}{2}+\frac{v'}{2}\right]\Sigma^a\left[p+\beta',q+\frac{\eta'}{2}\right] .&\end{aligned} \tag{30}$$

Using Eq. (25) applied to both sides of Eq. (30) we arrived, as we should, at the following result:

$$\Sigma^{\gtrless}(k,k')=\int d\delta\, d\eta\, \Sigma^{r}(k,\delta)G^{\gtrless}(\delta,\eta)\Sigma^{a}(\eta,k') \tag{31}$$

which, with random-impurity-distribution averaging and without external potential, yields

$$\Sigma^{><(k,k)}=n_i\int d\eta |T_{k\eta}|^2 G^{\gtrless}(\eta)\ , \tag{32}$$

where use is made here of the relation: $[\Sigma^r]^\dagger=\Sigma^a$. The above result is also given by Mahan.[7] For simulating quantum-based devices the self-energies must be calculated self-consistently using Eq. (30) or Eq. (31) together with Eq. (26). From Eqs. (6) and (30), we have

$$\Gamma(p,q)=\frac{1}{(h^4)^4}\int d\eta\, d\eta'\, d\beta\, d\beta'\, d\nu\, d\nu'\, dj\, dj' \exp\left[\frac{-i}{\hbar}(\beta\cdot\eta'+\beta'\cdot\eta+j\cdot\upsilon'+j'\cdot\upsilon)\right]$$
$$\times\Sigma^r\left[p+\beta+j,q-\frac{\eta}{2}-\frac{\nu}{2}\right]A\left[p+\beta+j',q-\frac{\eta}{2}+\frac{\nu'}{2}\right]\Sigma^a\left[p+\beta',j+\frac{\eta'}{2}\right]\ . \tag{33}$$

In momentum space, using Eqs. (6) and (31), the above equation reduces to an equation corresponding to Eq. (28),

$$\Gamma(k,k')=\int d\delta\, d\eta\, \Sigma^r(k,\delta)A(\delta,\eta)\Sigma^a(\eta,k')\ . \tag{34}$$

In applying to the general quantum-transport equation, Eq. (15), $\Sigma^<(p,q)$ and $\Gamma(p,q)$, which determine the kernel of integration, will have to be calculated self-consistently from Eqs. (30) and (33), respectively. The numerical implementation for doing the simulation will involve an iterative scheme to incorporate the necessary self-consistency, discussed in Sec. V.

B. Electron scattering with quantized "boson" wave field

The scattering of particles in a solid by a quantized "boson" wave field is generally described by second-quantized Hamiltonian operator having the general form[23–25]

$$H=H_P(\Psi^\dagger,\Psi)+H_F(\pi,\phi)+H_{PF}(\Psi^\dagger,\Psi,\pi,\phi)\ , \tag{35}$$

where

$$H_P(\Psi^\dagger,\Psi)=\sum_{\mathbf{R},\alpha}\Psi^\dagger_\alpha(\mathbf{R},t)E_\alpha\left[-\frac{\hbar}{i}\nabla_{\mathbf{R}}\right]\Psi_\alpha(\mathbf{R},t)\ , \tag{36}$$

$$H_F(\pi,\phi)=\sum_{\mathbf{R}}\frac{\pi^2(\mathbf{R},t)}{2\gamma}+\begin{cases}\frac{g}{2}|\nabla A|^2\\ \frac{g}{2}|\nabla_{\mathbf{R}}P(\mathbf{R},t)|^2\\ \frac{\gamma}{2}\omega^2P^2(\mathbf{R},t)\end{cases} \tag{37}$$

for electromagnetic field, acoustic phonons, and polar crystals, respectively,

$$H_{\rm PF}(\Psi^\dagger,\Psi,\pi,\phi)$$
$$=-\sum_{\mathbf{R},\alpha,\beta,i}\Psi^\dagger_\alpha(\mathbf{R},t)\gamma^i_{\alpha\beta}(\mathbf{R})\Psi_\beta(\mathbf{R},t)\begin{cases}P_i(\mathbf{R},t)\\ A_i(\mathbf{R},t)\end{cases} \tag{38}$$

for phonons and photons, respectively. $E_\alpha(k)$ is the energy-band function of Bloch electrons, and $\mathbf{R}$ denotes the lattice point coordinate.[13,14] For phonons in a solid, the scalar γ is related to the ratio of atomic mass to the effective charge of resulting dipole moments and g is related to the elastic constant of a lattice of atoms. The greek indices include all quantum labels. For the electromagnetic wave field, $\gamma=1/4\pi c^2$ and $g=1/4\pi$. The equal-time commutation rules for the field operators are as follows.

(a) For matter–wave-field operators,

$$\{\Psi^\dagger_\alpha(\mathbf{R},t),\Psi^\dagger_\beta(\mathbf{R}',t)\}=\{\Psi_\alpha(\mathbf{R},t),\Psi_\beta(\mathbf{R}',t)\}=0\ , \tag{39}$$

$$\{\Psi\alpha(\mathbf{R},t),\Psi^\dagger_\beta(\mathbf{R}',t)\}=\delta_{\alpha\beta}\delta_{\mathbf{R}\mathbf{R}'}\ . \tag{40}$$

(b) For phonon wave field $[\phi=P]$,

$$[\pi_l(\mathbf{R},t),P_j(\mathbf{R}',t)]=\frac{\hbar}{i}\delta_{lj}\delta_{RR'}\ , \tag{41}$$

$$[\pi_l(\mathbf{R},t),\pi_j(\mathbf{R}',t)]=[P_l(\mathbf{R},t),P_j(\mathbf{R}',t)]=0\ . \tag{42}$$

(c) For electromagnetic photon wave field $(\pi_l=\dot{A}_l/4\pi c^2)$,

$$[A_l(\mathbf{R},t),A_j(\mathbf{R}',t)]=[\pi_l(\mathbf{R},t),\pi_j(\mathbf{R},t)]=0\ , \tag{43}$$

$$[\pi_l(\mathbf{R},t),A_j(\mathbf{R}',t)]=\frac{\hbar}{i}\delta^T_{lj}\delta^T_{RR'}\ , \tag{44}$$

where $\delta^T_{lj}\delta^T_{\mathbf{R}\mathbf{R}'}$ is the so-called transverse δ function $(\nabla\cdot\mathbf{A}=0)$, which in the continuum limit is given by

$$\delta^T_{lj}(\mathbf{x}-\mathbf{x}')=\frac{1}{(h)^3}\int d\mathbf{k}\, e^{(i\mathbf{k}/\hbar)\cdot(\mathbf{x}-\mathbf{x}')}\left[\delta_{lj}-\frac{k_lk_j}{k^2}\right]\ . \tag{45}$$

Note the universal form of the interaction Hamiltonian operator given by Eq. (38), characterizing the interaction of quantized wave field with the particles. Indeed, the impurity scattering, discussed in Sec. IV A, interaction Hamiltonian operator can also be cast in the form of Eq. (38) (e.g., the Hamiltonian of the famous Kondo problem in dilute magnetic alloys).

The coupling matrix $\gamma^i_{\alpha\beta}(R)$ in Eq. (38) has the following expression for electrons in a solid. (a) For phonons

$$\gamma_{\alpha\beta}(\mathbf{R})=\int a^*_\alpha(\mathbf{x}-\mathbf{R})\left[\nabla_{\mathbf{R}}\frac{1}{|\mathbf{x}-\mathbf{R}|}\right]a_\beta(\mathbf{x}-\mathbf{R})d\mathbf{x}\ . \tag{46}$$

(b) For photons

$$\gamma_{\alpha\beta}(\mathbf{R})=\frac{e}{mc}\int a_\alpha^*(\mathbf{x}-\mathbf{R})\left[\frac{-\hbar}{i}\nabla_{\mathbf{x}}\right]a_\beta(\mathbf{x}-\mathbf{R})d\mathbf{x}\ . \quad (47)$$

(c) For electron-impurity scattering (given here for completeness)

$$\gamma_{\alpha\beta}(\mathbf{R})=\int a_\alpha^*(\mathbf{x}-\mathbf{R})\left[\frac{Z'e^2}{|\mathbf{x}-\mathbf{R}|}e^{-\sigma\cdot(\mathbf{x}-\mathbf{R})}\right]\times S_{\alpha\beta}a_\beta(\mathbf{x}-\mathbf{R})d\mathbf{x}\ , \quad (48)$$

where $a(\mathbf{x}-\mathbf{R})$ represents the localized Wannier function and $S_{\alpha\beta}$ is the Pauli matrix for the case of magnetic impurities.

In what follows, we will evaluate sums over lattice points as an integral (i.e., continuum approximation of the lattice coordinates, $\sum_{\mathbf{R}}\rightarrow\int d\mathbf{R}$). Dropping the greek indices, for simplicity (i.e., one-band model and spin-independent interactions), it is easy to see that the approximation to the electron self-energy for electron-phonon scattering is very similar to that which arises for electron-electron Coulomb interaction. In the electron-phonon interaction, the two-body potential is replaced by the phonon propagator $D_0(x_1x_2)$, multiplied by the square of the electron-phonon coupling constant. Thus the perturbation treatment of electron-phonon scattering is formally similar to that for the electron-electron interaction problems.[21]

A meaningful and significant contribution to the electron-phonon self-energy is given by a "one-phonon" diagram similar to the Hartree-Fock exchange diagram of the electron-electron scattering [note that in contrast to $V(x_1,x_2)$, the phonon propagator $D(x_1,x_2)$ is nonlocal in time] defined on the time contour as

$$\Sigma(1,2)=iG(1,2)D(1,2)\ . \quad (49)$$

Therefore by "fixing" the time order, we immediately obtain on real time axis,

$$\Sigma^{\gtrless}(1,2)=iG^{\gtrless}(1,2)D^{\gtrless}(1,2)\ . \quad (50)$$

Equation (50) immediately leads to the following expression for the retarded and advanced self-energies in terms of Green's function and phonon propagator as

$$\Sigma^{r,a}(1,2)=i[G^{r,a}(1,2)D^{>}(1,2)+G^{<}(1,2)D^{r,a}(1,2)]\ . \quad (51)$$

To avoid the immense complication of solving the complete quantum-transport equation for phonons to obtain the nonequilibrium phonon propagator, we make some simplifications. We may assume that we can use the phonon propagator for a phonon system at equilibrium. Note, however, that the phonon relaxation times may be comparable to the electron transit time across the quantum region of a device.[8-10]

In applying the above results for phonon scattering to Eq. (15), we are interested in the Weyl-transform equivalent of Eq. (50). We have, using four-dimensional vectors of Eq. (10), the following:

$$\Sigma^{\gtrless}(p,q)=i\int dv\, e^{(i/\hbar)p\cdot v}G^{\gtrless}(q-\tfrac{1}{2}v,q+\tfrac{1}{2}v)\times D^{\lessgtr}(q-\tfrac{1}{2}v,q+\tfrac{1}{2}v)\ . \quad (52)$$

The phonon propagator for a phonon system at equilibrium satisfies the following relation:

$$D^{\gtrless}(q-\tfrac{1}{2}v,q+\tfrac{1}{2}v)=D^{\gtrless}(v)\ , \quad (53)$$

$$D^{\gtrless}(v)=\frac{1}{h^4}\int dk\, e^{(i/\hbar)k\cdot v}D^{\gtrless}(k)\ . \quad (54)$$

Hence we have

$$\Sigma^{\gtrless}(p,q)=\frac{i}{h^4}\int dk\, dv e^{(i/\hbar)(p+k)\cdot v}\times G^{\gtrless}(q-\tfrac{1}{2}v,q+\tfrac{1}{2}v)D^{\gtrless}(k)=\frac{i}{h^4}\int dk\, G^{\gtrless}(p+k,q)D^{\gtrless}(k)\ . \quad (55)$$

and therefore, we also have

$$\Gamma(p,q)=-\frac{1}{h^4}\int dk[G^{>}(p+k,q)D^{>}(k)-G^{<}(p+k,q)D^{<}(k)]\ . \quad (56)$$

Equations (55) and (56) are general relations within the one-photon diagram approximation to the self-energy. If we use the δ-function approximation to the spectral weight function for phonons and write the expression for the Fourier-transformed equilibrium phonon propagator as

$$D^{<}(\mathbf{k},E')=-i\gamma_{\mathbf{k}}^2[(N_{\mathbf{k}}+1)\delta(E'-\Omega_{\mathbf{k}})+N_{\mathbf{k}}\delta(E'+\Omega_{\mathbf{k}})]\ , \quad (57)$$

$$D^{>}(\mathbf{k},E')=-i\gamma_{\mathbf{k}}^2[(N_{\mathbf{k}}+1)(E'+\Omega_{\mathbf{k}})+N_{\mathbf{k}}\delta(E'-\Omega_{\mathbf{k}})]\ , \quad (58)$$

where Ω_k is the energy-momentum relation for phonons, then substitute the explicit expression for $D^{>}(\mathbf{k},E')$ and $D^{<}(\mathbf{k},E')$ in the expression for $\Sigma^{\gtrless}(p,q)$ and $\Gamma(p,q)$ above and integrate with respect to E', we obtain the following expressions:

$$\Sigma^{<}(p,q)=\frac{1}{h^3}\int d\mathbf{k}[G^{<}(\mathbf{p}+\mathbf{k},E+\Omega_{\mathbf{k}},q)\gamma_{\mathbf{k}}^2(N_{\mathbf{k}}+1)+G^{<}(\mathbf{p}+\mathbf{k},E-\Omega_{\mathbf{k}},q)\gamma_{\mathbf{k}}^2N_{\mathbf{k}}]\ , \quad (59)$$

$$\Sigma^{>}(p,q)=\frac{1}{h^3}\int d\mathbf{k}\, G^{>}(\mathbf{p}+\mathbf{k},E-\Omega_{\mathbf{k}},q)\gamma_{\mathbf{k}}^2(N_{\mathbf{k}}+1)+G^{>}(\mathbf{p}+\mathbf{k},E+\Omega_{\mathbf{k}},q)\gamma_{\mathbf{k}}^2N_{\mathbf{k}}\ , \quad (60)$$

$$\Gamma(p,q)=\frac{1}{h^3}\int d\mathbf{k}\{\gamma_{\mathbf{k}}^2N_{\mathbf{k}}[A(\mathbf{p}+\mathbf{k},E+\Omega_{\mathbf{k}},q)+A(\mathbf{p}+\mathbf{k},E-\Omega_{\mathbf{k}},q)]+i\gamma_{\mathbf{k}}^2[G^{>}(\mathbf{p}+\mathbf{k},E-\Omega_{\mathbf{k}},q)-G^{<}(\mathbf{p}+\mathbf{k},E+\Omega_{\mathbf{k}},q)]\}\ . \quad (61)$$

We note that for uniform systems at steady-state condi-

tions (independent of q), use can be made of the following exact relations:

$$-iG^{<}(\mathbf{p},E)=f(\mathbf{p},E)A(\mathbf{p},\mathbf{E}) , \tag{62}$$

$$iG^{>}(\mathbf{p},\mathbf{E})=[1-f(\mathbf{p},\mathbf{E})]A(\mathbf{p},\mathbf{E}) , \tag{63}$$

where

$$\frac{1}{h}\int dE\ A(\mathbf{p},E)=1 ,$$

which follows from equal-time commutation relations for the field operators. These relations are exact since the Weyl transform of the product of operators for uniform system at steady state reduces to the product of their Weyl transforms. However, for nonuniform systems and/or nonstationary states, these relations do not hold and the so-called "Kadanoff-Baym ansatz"[1,6,26] are not generally valid for nonequilibrium transport. The Kadanoff-Baym ansatz is valid only up to the first order in the gradient (i.e., has zero-order accuracy) and the so-called "generalized Kadanoff-Baym ansatz" given by Lipavsky, Spicka, and Velicky[26] can be shown to be valid only up to the second order in the gradient expansions (Appendix C). When the last two relations are substituted in the expression for $\Sigma^{<}(p,q)$ and $\Gamma(p,q)$ we obtain

$$\Sigma^{<}(p,q)=\frac{i}{h^3}\int d\mathbf{k}\, f(\mathbf{p}+\mathbf{k},E+\Omega_{\mathbf{k}}) \times A(\mathbf{p}+\mathbf{k},E+\Omega_{\mathbf{k}})\gamma_k^2(N_{\mathbf{k}}+1) +f(\mathbf{p}+\mathbf{k},E-\Omega_{\mathbf{k}})A(\mathbf{p}+\mathbf{k},E-\Omega_{\mathbf{k}})\gamma_{\mathbf{k}}^2 N_{\mathbf{k}} , \tag{64}$$

$$\Gamma(p,q)=\frac{1}{h^3}\int d\mathbf{k}\{\gamma_{\mathbf{k}}^2[N_{\mathbf{k}}+f(\mathbf{p}+\mathbf{k},E+\Omega_{\mathbf{k}})] \times A(\mathbf{p}+\mathbf{k},E+\Omega_{\mathbf{k}}) +\gamma_{\mathbf{k}}^2[N_{\mathbf{k}}+1-f(\mathbf{p}+\mathbf{k},E-\Omega_{\mathbf{k}})] \times A(\mathbf{p}+\mathbf{k},E-\Omega_{\mathbf{k}})\} , \tag{65}$$

which agrees with the result given by Mahan.[7] For application to the simulation of high-speed devices using Eq. (15), the more general results will have to be used self-consistently through an iterative numerical procedure.

V. SELF-CONSISTENT SOLUTION AND SIMPLIFICATIONS OF MANY-BODY QUANTUM-TRANSPORT EQUATIONS

The exact quantum-transport equation, Eq. (15), does not stand alone for a couple of reasons: (a) this equation is coupled to the equation for G^r (or $G^>$) and to the boson field propagators, and (b) the kernel of the integral operators depends on G^r (or $G^>$) and the solution $G^<$ (and hence f_w), as weli as, in general, to the boson field propagators. In Sec. IV B, we made the assumption that the phonon propagator is known and corresponds to the propagator for a phonon system at equilibrium. Besides the approximations made in the self-energy expressions, this constitutes one major simplification of Eq. (15), by giving up self-consistency with respect to the phonon (or interacting boson) systems.

However, self-consistency with respect to the particle system must at least be retained. Following the well-known standard technique of all many-body calculations, one tries to achieve self-consistency by an iterative procedure. Therefore, to solve Eq. (15) one uses "noninteracting" $G_0^<$ and G_0^r (or $G_0^>$) to evaluate the kernel of the integral operator, and all other terms on the RHS of this equation [note that $H(p,q)$ includes $\mathrm{Re}\Sigma^r(p,q)$]. Then the known"operators" in the RHS of Eq. (15) are used to solve for new $G^<$ and f_w. The equation for G^r, Eq. (8), will also be solved for a new G^r after which the process may be repeated with the new approximate $G^<$ and G^r.

In the practical numerical simulation of quantum-based devices, the first iteration of the above-mentioned self-consistency procedure may represent a more sufficiently accurate solution, depending on the choice of the starting solutions for the iteration process. A clear choice for quantum-based device analysis would be the solutions obtained for noninteracting particles. This means that the zero-order approximation neglects all the terms except the first term in the RHS of Eq. (15). The numerical procedure and technique for obtaining time-dependent and steady-state solutions for a resonant-tunneling device, within the effective-mass approximation for noninteracting particles, is described in Sec. III. The "zero-order" Green's functions may then be taken to correspond to the solution of Eq. (21), discussed in Sec. III. A first step towards real calculations which account for full quantum effects and many-body effects, using the relaxation-time approximation, is undertaken in Sec. VII, which already yields remarkably new and physically meaningful results. Further comments are given at the end of the paper.

VI. QUANTUM-TRANSPORT EQUATIONS FOR UNIFORM EXTERNAL ELECTRIC FIELDS

The area of quantum transport in solids under very high external electromagnetic fields has received much attention in recent years.[4–7] In this section we will give a demonstration of the power of the lattice Weyl-Wigner formalism of quantum transport in doing analytical calculations on this problem. Indeed the formalism presented here enables us to formulate the exact equation in a straightforward and fully gauge-invariant manner, without the need to perform a gradient expansion. Most treatments of this problem in the literature are not fully and rigorously gauge invariant, and proceed as a gradient expansion from the very beginning.

We consider a crystalline solid as a translationally invariant electron-phonon scattering system at equilibrium. Then the electron spectral weight function in the absence of an external electric field $A(\mathbf{p}_0,z_0)$ is given by

$$A(\mathbf{p}_0,z_0)=\frac{\Gamma(\mathbf{p},z_0)}{[z_0-E_\alpha(\mathbf{p}_0)-\mathrm{Re}\Sigma^r(\mathbf{p}_0,z_0)]^2+\left[\frac{\Gamma(\mathbf{p}_0,z_0)}{2}\right]^2}, \tag{66}$$

where z_0 is the energy variable in the absence of the field, $E_\alpha(\mathbf{p})$ incorporates the Hartree-Fock approximation to the self-energy and $\Gamma(\mathbf{p}_0,z_0)$ may be given by Eq. (65). The expression for $\Sigma^r(\mathbf{p}_0,z_0)$, using Eq. (65), is

$$\Sigma^r(\mathbf{p}_0,z_0)=\int\frac{dE'}{2\pi}\frac{\Gamma(\mathbf{p}_0,E')}{z_0+i\epsilon-E'}. \tag{67}$$

From the looks of Eqs. (66) and (67), it clear that, in general, a many-body calculation involves what is often termed as a "bootstrap process" to obtain self-consistent solutions for $\Sigma^r(\mathbf{p}_0,z_0),\Gamma(\mathbf{p}_0,z_0),A(\mathbf{p}_0,z_0),G^r(\mathbf{p}_0,z_0)$, etc. For the purpose of the present demonstration, we assume that in the absence of the electric field, the self-energies and Green's functions are found self-consistently, to some degree of approximation.

The time-evolution equations for $G^{r,a}(1,1')$ are obtained by converting Eqs. (A5) and (A6) to the real-time axis, which yield the following:

$$\int d2(G^{r,a})^{-1}(1,2)G^{r,a}(2,1')=\delta(1-1'), \tag{68}$$

$$\int d2G^{r,a}(1,2)[G^{r,a}(2,1')]^{-1}=\delta(1-1'), \tag{69}$$

when $[G^{r,a}(1,1')]^{-1}$ is defined by

$$[G^{r,a}(1,1')]^{-1}=\left[i\hbar\frac{\partial}{\partial t_1}-E_\alpha\left[-\frac{\hbar}{i}\nabla_1\right]\right]\delta(1-1')-\Sigma^{r,a}(1,1'). \tag{70}$$

The resulting homogeneous differential equations corresponding to Eqs. (68) and (69) define an "effective time-dependent Schrödinger equation" and its adjoint (transpose in matrix terminology) equation, respectively. The corresponding time-independent homogeneous differential equations in turn define Schrödinger eigenvalue equations with nonlocal and energy-dependent potentials for the operators $\mathcal{L}(z_0)$ and its adjoint $\tilde{\mathcal{L}}(z_0)$, or the left- and right-eigenvector equations for $\mathcal{L}(z_0)$,

$$\mathcal{L}(z_0)\phi_n(z_0)=W_n(z_0)\phi_n(z_0), \tag{71}$$

$$\tilde{\mathcal{L}}(z_0)\eta_m(z_0)=W_m(z_0)\eta_m(z_0)=\eta_m^T(z_0)L(z_0), \tag{72}$$

where the non-Hermitian operator $\mathcal{L}(z_0)$ is given by

$$\mathcal{L}^{r,a}(1,1',z_0)=E_\alpha\left[-\frac{\hbar}{i}\nabla_1\right]\delta(1-1')+\mathrm{Re}\Sigma^{r,a}(1,1',z_0)\pm\frac{i\Gamma}{2}(1,1',z_0). \tag{73}$$

Assuming that the eigenvalues are distinct, $\phi_n(z_0)$ and $\eta_m(z_0)$ form a biorthogonal system. It is more convenient in quantum mechanics to consider the Hermitian adjoint eigenvalue equation

$$\mathcal{L}^\dagger(z_0)\psi_m(z_0)=W_m^*(z_0)\psi_m(z_0), \tag{74}$$

so that the dual set biorthogonal to $\{\phi_n(z_0)\}$ is the set $\{\psi_m^*(z_0)\}$, and the resulting formalism using these eigenvectors closely parallels those for Hermitian operators [note that the eigenvalues corresponding to $\phi_n(z_0)$ and $\psi_n^*(z_0)$ are identical]. By virtue of the "average" perfect periodicity that is present in the effective Schrödinger equation, we will refer to the eigenvector $\phi_n(z_0)$ and $\psi_n^*(z_0)$ as the biorthogonal pairs of Bloch functions $b_\alpha(\mathbf{x},\mathbf{p}_0,z_0)$ and $b_\alpha^*(\mathbf{x},\mathbf{p}_0,z_0)$, respectively. Their respective lattice fourier transforms are similarly defined as the biorthogonal pairs of Wannier functions $a_\alpha(\mathbf{x}-\mathbf{q},z_0)$ and $a_\alpha^*(\mathbf{x}-\mathbf{q},z_0)$, respectively. The one-particle "renormalized" energy band $\tilde{E}_\alpha$ belonging to band index α is, in the quasiparticle picture, given by the solution of

$$\tilde{E}_\alpha-W_\alpha(\mathbf{p}_0,\tilde{E}_\alpha)=0, \tag{75}$$

where $W_\alpha(\mathbf{p}_0,\tilde{E}_\alpha)=E_\alpha(\mathbf{p}_0)+\Sigma_\alpha^r(\mathbf{p}_0,\tilde{E}_\alpha)$. These zero-field solutions provide a good starting point for generalization in the presence of external electromagnetic field.

In the presence of high uniform electric field $\mathbf{F}$, the perfect periodicity of the system is destroyed and hence the zero-field biorthogonal Bloch functions and its corresponding zero-field biorthogonal Wannier functions cease to be convenient basis states for formulating the Weyl-Wigner quantum dynamics. The proper biorthogonal basis states can be determined with the help of the gauge-invariant shift or translation operators $T(\mathbf{q})$, where $T(\mathbf{q})$ is the lattice translation. With the Hamiltonian given by $\mathcal{H}=\mathcal{H}_0-e\mathbf{F}\cdot\mathbf{x}$, where $\mathcal{H}_0$ is the periodic part in the absence of the field, we have

$$\dot{T}(q)=\frac{i}{\hbar}[\mathcal{H},T(\mathbf{q})]=\frac{i}{\hbar}e\mathbf{F}\cdot\mathbf{q}\ T(q). \tag{76}$$

This means that $[\mathcal{H},T(\mathbf{q})]$ is diagonal in the bilinear expansion if $T(\mathbf{q})$ is also "bidiagonal." The eigenfunction of the lattice translation operator $T(\mathbf{q})$ must then be labeled by a wave number $\mathbf{k}$ which is varying in time as

$$\mathbf{k}=\mathbf{k}_0+\frac{e\mathbf{F}}{\hbar}t. \tag{77}$$

This means that $\mathcal{H}$ is also diagonal in $\mathbf{k}$. The electric Bloch function $B_\alpha(\mathbf{k},\mathbf{r})$ may be considered to be the eigenfunction of $T(\mathbf{q})$. From the usual lattice Fourier-transform relation, the corresponding basis states labeled by lattice and time coordinates (Dirac δ-function basis for time variable) acquire "Peierl phase factors," i.e., in the continuum approximation, we have

$$\langle q-\tfrac{1}{2}v|_F\Longrightarrow\exp\left[\frac{ie}{\hbar}\mathbf{F}(t-\tfrac{1}{2}\tau)\cdot(\mathbf{q}-\tfrac{1}{2}\mathbf{v})\right]\langle q-\tfrac{1}{2}v|_0, \tag{78}$$

$$|q+\tfrac{1}{2}v\rangle_F \Longrightarrow \exp\left[\frac{ie}{\hbar}\mathbf{F}(t+\tfrac{1}{2}\tau)\cdot(\mathbf{q}+\tfrac{1}{2}\mathbf{v})\right]|q+\tfrac{1}{2}v\rangle_0 , \tag{79}$$

where we have adopted the (3+1)-dimensional notation for q, i.e., $q\equiv(\mathbf{q},t)$. Thus, nonlocal quantities in space and time acquire phase factors in the presence of the field, such as

$$\langle q_1,|\hat{\Sigma}|q_2\rangle_F \Longrightarrow e^{-(ie/\hbar)\mathbf{F}t\cdot(\mathbf{q}_1-\mathbf{q}_2)}e^{-(ie/\hbar)\mathbf{F}\cdot\mathbf{q}(t_1-t_2)} \times\Sigma_0(\mathbf{q}_1-\mathbf{q}_2,t_1-t_2) , \tag{80}$$

where $\mathbf{q}=(\mathbf{q}_1+\mathbf{q}_2)/2$ and $t=(t_1+t_2)/2$. Therefore, besides the wave number varying in time given by Eq. (77), the energy variable z_0 in the absence of the field now varies with the lattice coordinate $\mathbf{q}$ as

$$z_0\rightarrow z_0+e\mathbf{F}\cdot\mathbf{q}=z . \tag{81}$$

The eigenfunctions of the gauge-invariant translations operator which now form the biorthogonal system of electric Bloch functions, $B(\mathbf{x},\mathbf{k},z)$ and $B^*(x,\mathbf{k},z)$, are determined from the eigenvectors[27] of $L(z)$ and its adjoint $L^\dagger(z)$

$$L(z)B_\alpha(\mathbf{x},\mathbf{k},z)=W_\alpha(\mathbf{k},z)B_\alpha(\mathbf{x},\mathbf{k},z) , \tag{82}$$

$$L^\dagger(z)\psi_m(\mathbf{x},\mathbf{k},z)=W_m^*(\mathbf{k},z)\psi_m(\mathbf{x},\mathbf{k},z) , \tag{83}$$

where $B_\alpha^*(\mathbf{x},\mathbf{k},z)=\psi_m^*(\mathbf{x},\mathbf{k},z)$, $W_\alpha(\mathbf{k},z)=E_\alpha(\mathbf{k})+\Sigma'(\mathbf{k},z)$, and

$$L(z)=\mathcal{L}(z)-e\mathbf{F}\cdot\left[\mathbf{x}+i\frac{\partial}{\partial\mathbf{k}}\right] , \tag{84}$$

$$B_\alpha(\mathbf{x},\mathbf{k},z)=b_\alpha\left[\mathbf{x},\mathbf{k}_0+\frac{e\mathbf{F}t}{\hbar},z_0+e\mathbf{F}\cdot\mathbf{q}\right] , \tag{85}$$

$$W_\alpha(\mathbf{k},z)=W_\alpha\left[\mathbf{k}_0+\frac{e\mathbf{F}t}{\hbar},z_0+e\mathbf{F}\cdot\mathbf{q}\right] . \tag{86}$$

The corresponding set of biorthogonal electric Wannier functions are given by the lattice Fourier transformation, with the transformation function given, as usual, by

$$\langle A_\alpha(\mathbf{q},z)|B_\alpha(\mathbf{k},z)\rangle=\frac{1}{(N\hbar^3)^{1/2}}e^{i\mathbf{k}_0\cdot\mathbf{q}} , \tag{87}$$

where $N\hbar^3$ goes to h^3 in the continuum limit. The above results are completely analogous to the results obtained for an external uniform magnetic field.[14] Indeed, by writing the vector potential for a general case as $\mathbf{A}=\frac{1}{2}(\mathbf{B}\times\mathbf{r})-c\mathbf{F}\mathbf{t}$, we have the following expression for the electromagnetic Bloch function and Wannier function for a single band, which takes account of the presence of other bands through the explicit dependence in the fields beyond the Peierls phase factor,

$$B_\alpha(\mathbf{x},\mathbf{k},z)=b_\alpha\left[\mathbf{x},\mathbf{k}_0-\frac{1}{2}\frac{e}{\hbar c}\mathbf{A},z_0+e\mathbf{F}\cdot\mathbf{q},\mathbf{F},\mathbf{B}\right] , \tag{88}$$

$$A_\alpha(\mathbf{x},\mathbf{q},z)=e^{-(1/2)(ie/\hbar c)\mathbf{A}\cdot\mathbf{q}}a_\alpha(\mathbf{x}-\mathbf{q},z_0+e\mathbf{F}\cdot\mathbf{q},\mathbf{F},\mathbf{B}) , \tag{89}$$

which reduces to the appropriate expression for the electric or magnetic field case.[13,14]

By virtue of the commutation of $[\mathcal{H},T(\mathbf{q})]$, we seek solutions of $\mathcal{H}$ which diagonalize $T(\mathbf{q})$. These allow us to search for the solution of the time-dependent effective Schrödinger equation, where the time dependence enters solely from Eq. (77). Therefore we seek a solution to an effective time-dependent Schrödinger equation as

$$(\mathcal{L}-e\mathbf{F}\cdot\mathbf{x})\psi_a(\mathbf{x},t)=i\hbar\frac{\partial\psi_\alpha(\mathbf{x},t)}{\partial t} ,$$

which may now be written as

$$(\mathcal{L}-e\mathbf{F}\cdot\mathbf{x})\psi_\alpha(\mathbf{x},\mathbf{k})=ie\mathbf{F}\cdot\frac{\partial\psi_\alpha(\mathbf{x},\mathbf{k})}{\partial\mathbf{k}} , \tag{90}$$

and its Hermitian adjoint. Writing

$$\psi_\alpha(\mathbf{x},\mathbf{k})=f(\mathbf{k})B_\alpha(\mathbf{x},\mathbf{k},z) , \tag{91}$$

we find, upon substituting in Eq. (90),

$$f(\mathbf{k})=\exp\left[\frac{-i}{eF}\int_{k_0}^{k_0+e\mathbf{F}t/\hbar}W_\alpha(\mathbf{k},z)d\mathbf{k}\right] =\exp\left[\frac{-i}{\hbar}\int_0^t W_\alpha(\mathbf{k}_0+e\mathbf{F}\tau')d\tau'\right] . \tag{92}$$

We now have all we need to calculate the many-body nonequilibrium Green's function. For simplicity we retain the one-band description. We expand the electron field operators in terms of $\psi_\alpha(\mathbf{x},\mathbf{k})$ and the complex conjugate of the Hermitian adjoint solution, $\psi_\alpha^*(\mathbf{x},\mathbf{k})$,

$$\hat{\psi}_\alpha(\mathbf{x},\mathbf{t})=\sum_{\mathbf{k}}\hat{C}_{\mathbf{k}}\psi_\alpha(\mathbf{x},\mathbf{k}) , \tag{93}$$

$$\hat{\psi}_\alpha^\dagger(\mathbf{x},t)=\sum_{\mathbf{k}'}\hat{C}_{\mathbf{k}'}^\dagger\psi_\alpha^*(\mathbf{x},\mathbf{k}') , \tag{94}$$

where $\hat{C}_{\mathbf{k}}$ and $\hat{C}_k^\dagger$ are the annihilation and creation operator, respectively. We construct $G^>(\mathbf{x},t,\mathbf{x}',t')$ (in what follows we will drop the index α) as

$$G^>(\mathbf{x},t,\mathbf{x}',t')=\frac{-i}{\hbar}\left\langle\sum_{\mathbf{k}}\hat{C}_{\mathbf{k}}\psi(\mathbf{x},\mathbf{k})\sum_{\mathbf{k}'}\hat{C}_{k'}^\dagger\psi^*(x,\mathbf{k}')\right\rangle =\frac{-i}{\hbar}\sum_{\mathbf{k}}\psi(\mathbf{x},\mathbf{k})\psi^*(x',\mathbf{k})[1-f_w(\mathbf{k})] . \tag{95}$$

Equation (95) can be written as an equation for the operator $G_{\rm op}^>(t,t')$ as

$$G^{>}_{\rm op}(t,t')=\frac{-i}{\hbar}\sum_{\mathbf{k}}\exp\left[\frac{-i}{e\mathbf{F}}\int_{\mathbf{k}-e\mathbf{F}t/\hbar}^{\mathbf{k}-e\mathbf{F}t'/\hbar}W(\mathbf{k}',z)d\mathbf{k}'\right]|B(\mathbf{k})\rangle\langle B(\mathbf{k})|[1-f_w(\mathbf{k})]\ . \tag{96}$$

We need the lattice Weyl transform of $G^{>}_{\rm op}(t,t')$. This is given in four-dimensional vector space as

$$G^{>}(p,q)=\frac{-i}{\hbar}\sum_{\mathbf{v},\tau,\mathbf{k}}e^{(i/\hbar)\mathbf{p}\cdot\mathbf{v}}e^{(i/\hbar)z_0\tau}\langle\mathbf{q}-\tfrac{1}{2}\mathbf{v},t-\tfrac{1}{2}\tau|B(\mathbf{k})\rangle\langle B(\mathbf{k})|\mathbf{q}+\tfrac{1}{2}v,t+\tfrac{1}{2}\tau\rangle$$
$$\times[1-f_w(\mathbf{k})]\exp\left[\frac{-i}{e\mathbf{F}}\int_{\mathbf{k}-e\mathbf{F}t/\hbar}^{\mathbf{k}-e\mathbf{F}t'/\hbar}W(\mathbf{k}',z)d\mathbf{k}'\right]\ . \tag{97}$$

Using Eq. (87) in Eq. (97), we obtain, after carrying the summation over $\mathbf{v}$ and $\mathbf{k}$, the following expression ($\Sigma_\tau\rightarrow\int d\tau$):

$$G^{>}(p,q)=\frac{-i}{\hbar}\int d\tau\, e^{(i/\hbar)(z_0+e\mathbf{F}\cdot\mathbf{q})\tau}\exp\left[\frac{-i}{\hbar}\int_{-\tau/2}^{\tau/2}\mathrm{Re}W(\mathbf{p}+e\mathbf{F}\tau',z)d\tau'\right][1-f_w(\mathbf{p}+e\mathbf{F}t)]$$
$$\times\exp\left[\frac{-1}{2\hbar}\int_{-|\tau|/2}^{|\tau|/2}\Gamma(\mathbf{p}+e\mathbf{F}\tau',z)d\tau'\right]\ . \tag{98}$$

By similar procedure, we find for $G^{<}(p,q)$ the result

$$G^{<}(p,q)=\frac{i}{h}\int d\tau\, e^{(i/\hbar)(z_0+e\mathbf{F}\cdot\mathbf{q})\tau}\exp\left[\frac{-i}{\hbar}\int_{-\tau/2}^{\tau/2}\mathrm{Re}W(\mathbf{p}+e\mathbf{F}\tau',z)d\tau'\right]f_w(\mathbf{p}+e\mathbf{F}t)$$
$$\times\exp\left[\frac{-1}{2\hbar}\int_{-|\tau|/2}^{|\tau|/2}\Gamma(\mathbf{p}+e\mathbf{F}\tau',z)d\tau'\right]\ . \tag{99}$$

The electron spectral-weight function $A(p,q)$ is therefore given by

$$A(p,q)=\int d\tau\, e^{(i/\hbar)(z_0+e\mathbf{F}\cdot\mathbf{q})\tau}\exp\left[\frac{-i}{\hbar}\int_{-\tau/2}^{\tau/2}\mathrm{Re}W(\mathbf{p}+e\mathbf{F}\tau',z)d\tau'\right]\exp\left[-\frac{1}{2\hbar}\int_{-|\tau|/2}^{|\tau|/2}\Gamma(\mathbf{p}+e\mathbf{F}\tau',z)d\tau'\right]\ . \tag{100}$$

We immediately observe that in the limit $F\rightarrow 0$, Eq. (100) for $A(\mathbf{p},q)$ correctly reduces to the zero-field expression given by Eq. (66). Note that we have also shown here for the first time, in a gauge-invariant manner, the exact validity of the Kadanoff-Baym *ansatz* [Eqs. (98) and (99)] for Bloch electrons in a uniform electric field; this has been suspected to be true for some time (although debated in the literature).

We are now in the position to write down the "nongradient" expression for the quantum many-body transport equation for high electric fields. First we observe the functional dependence of all quantities appearing in Eq. (14). Writing $z=E+e\mathbf{F}\cdot q$, $\mathbf{K}=p+e\mathbf{F}t$, we have

$$H(p,q)=E_\alpha(\mathbf{K})+\mathrm{Re}\Sigma^r(\mathbf{K},z)-e\mathbf{F}\cdot\mathbf{q}\ , \tag{101}$$

$$G^{<}(p,q)=G^{<}(\mathbf{p},\mathbf{K},z),\quad A(p,q)=A(\mathbf{p},z),\quad \Gamma(p,q)=\Gamma(\mathbf{p},z)\ . \tag{102}$$

Therefore the Poisson bracket operator is given by

$$\hat{\Lambda}=\frac{\hbar}{z}\left[\left[\frac{\partial^{(a)}}{\partial\mathbf{q}}\cdot\frac{\partial^{(b)}}{\partial\mathbf{p}}-\frac{\partial^{(a)}}{\partial\mathbf{p}}\cdot\frac{\partial^{(b)}}{\partial\mathbf{q}}\right]+\left[\frac{\partial^{(a)}}{\partial t}\frac{\partial^{(b)}}{\partial E}-\frac{\partial^{(a)}}{\partial E}\frac{\partial^{(b)}}{\partial t}\right]\right]$$
$$=\frac{\hbar}{2}\left[\frac{\partial^{(a)}}{\partial\mathbf{q}}\cdot\frac{\partial^{(b)}}{\partial\mathbf{p}}-\frac{\partial^{(a)}}{\partial\mathbf{p}}\cdot\frac{\partial^{b}}{\partial\mathbf{q}}\right]+\frac{\partial E}{\partial\mathbf{q}}\cdot\left[\frac{\partial^{(a)}}{\partial E}\frac{\partial^{(b)}}{\partial\mathbf{p}}-\frac{\partial^{(a)}}{\partial p}\frac{\partial^{(b)}}{\partial E}\right]+\frac{\hbar}{2}\frac{\partial\mathbf{K}}{\partial t}\cdot\left[\frac{\partial^{(a)}}{\partial\mathbf{K}}\frac{\partial^{(b)}}{\partial E}-\frac{\partial^{(a)}}{\partial E}\frac{\partial^{(b)}}{\partial\mathbf{K}}\right]\ , \tag{103}$$

where the first term operates only on $\mathbf{q}$ which does not occur in the combination $z=E+e\mathbf{F}\cdot\mathbf{q}$. Noting that $\partial E/\partial\mathbf{q}=-e\mathbf{F}$ and $\partial\mathbf{K}/\partial t=e\mathbf{F}$ and substituting, we have

$$\hat{\Lambda}=\Lambda_1+\frac{\hbar}{2}e\mathbf{F}\cdot\left[\frac{\partial^{(a)}}{\partial\mathbf{p}}\frac{\partial^{(b)}}{\partial E}-\frac{\partial^{(a)}}{\partial E}\frac{\partial^{(b)}}{\partial\mathbf{p}}\right]\ , \tag{104}$$

where Λ_1 operates only on explicit functions of $\mathbf{q}$ (i.e., not in combination with E)

Therefore, Eq. (14) becomes

$$\frac{\partial G^<(p,q)}{\partial t}=-e\mathbf{F}\cdot\frac{\partial G^<(p,q)}{\partial \mathbf{p}}+\frac{2}{\hbar}\sin\hat{\Lambda}'[H(p,q)G^<(p,q)+\Sigma^<(p,q)\mathrm{Re}\hat{G}(p,q)]$$
$$+\frac{1}{\hbar}\cos\hat{\Lambda}'[\Sigma^<(p,q)A(p,q)-\Gamma(p,q)G^<(p,q)]\ , \tag{105}$$

where $\hat{\Lambda}'$ is given by the last term of Eq. (104) and

$$H(p,q)=E_\alpha(\mathbf{p}+e\mathbf{F}t)+\mathrm{Re}\Sigma^r_\alpha(\mathbf{p}+e\mathbf{F}t,E+e\mathbf{F}\cdot\mathbf{q})\ .$$

The corresponding integro-differential quantum-transport equation is

$$\frac{\partial G^<}{\partial t}(p,q)=e\mathbf{F}\cdot\frac{\partial G^<}{\partial \mathbf{p}}(p,q)+\frac{2}{(h^4)^2}\int d\mathbf{p}'dE'K^S_H(\mathbf{p},E-E';E,\mathbf{p}-\mathbf{p}')G^<(\mathbf{p}',E')$$
$$+\frac{2}{(h^4)^2}\int d\mathbf{p}'dE'K^S_{\Sigma^<}(\mathbf{p},E-E';E,\mathbf{p}-\mathbf{p}')\mathrm{Re}G^r(\mathbf{p}',E')$$
$$-\frac{2}{(h^4)^2}\int d\mathbf{p}'dE'K^c_{\Sigma^<}(\mathbf{p},E-E';E,\mathbf{p}-\mathbf{p}')\mathrm{Im}G^r(\mathbf{p}',E')$$
$$-\frac{1}{(h^4)^2}\int d\mathbf{p}'dE'K^c_\Gamma(\mathbf{p},E-E';E,\mathbf{p}-\mathbf{p}),G^<(\mathbf{p}',E')\ , \tag{106}$$

where

$$K^s_a(\mathbf{p},E-E';E,\mathbf{p}-\mathbf{p}')=\int d\mathbf{v}\,dj\exp\left[\frac{2i}{\hbar}j(E-E')\right]\left[a\left[\mathbf{p}-e\mathbf{F}j,E+e\mathbf{F}\cdot\frac{\mathbf{v}}{2}\right]-a\left[p+e\mathbf{F}j,E-e\mathbf{F}\cdot\frac{\mathbf{v}}{2}\right]\right]$$
$$\times\sin\left[\frac{\mathbf{p}-\mathbf{p}'}{\hbar}\cdot\mathbf{v}\right]\ , \tag{107}$$

$$K^c_a(\mathbf{p},E-E';E,\mathbf{p}-\mathbf{p}')=\int d\mathbf{v}\,dj\exp\left[\frac{2i}{\hbar}j(E-E')\right]\left[a\left[\mathbf{p}-e\mathbf{F}j,E+e\mathbf{F}\cdot\frac{\mathbf{v}}{2}\right]+a\left[\mathbf{p}+e\mathbf{F}j,E-e\mathbf{F}\cdot\frac{\mathbf{v}}{2}\right]\right]$$
$$\times\cos\left[\frac{\mathbf{p}-\mathbf{p}'}{\hbar}\cdot\mathbf{v}\right]\ . \tag{108}$$

To the authors' knowledge Eqs. (105) and (106) for uniform external electric fields, which correspond to Eqs. (14) and (15), respectively, have not been given in the literature. If we expand (105) to first order in the gradient, we immediately obtain

$$\frac{\partial G^<(p,q)}{\partial t}+e\mathbf{F}\cdot\left[1+\frac{\partial}{\partial E}\mathrm{Re}\Sigma^r(p,q)\right]\frac{\partial G^<(p,q)}{\partial \mathbf{p}}-e\mathbf{F}\cdot\left[\frac{\partial E_\alpha(\mathbf{K})}{\partial \mathbf{p}}+\frac{\partial}{\partial \mathbf{p}}\mathrm{Re}\Sigma^r(p,q)\right]\frac{\partial G^<(p,q)}{\partial E}$$
$$-e\mathbf{F}\cdot\left[\frac{\partial\Sigma^<(p,q)}{\partial \mathbf{p}}\frac{\partial\mathrm{Re}G^<(p,q)}{\partial E}-\frac{\partial\Sigma^<(p,q)}{\partial E}\frac{\partial\mathrm{Re}G^r}{\partial \mathbf{p}}\right]=\frac{1}{h}\Sigma^<(p,q)A(p,q)-\Gamma(p,q)G^<(p,q) \tag{109}$$

Replacing $\partial/\partial E$, exhibited in the last equation, by $-\partial/\partial E$ (to account for differences in defining the space-time Fourier transform), the above result is identical to the result given by Mahan[7] to terms linear in the electric field. However, in the present case Eq. (109) is still highly nonlinear in the electric field through the functional dependence of the quantities appearing in the equation, as displayed in Eqs. (101) and (102).

We now calculate the collision terms on the RHS of Eq. (109) for phonon scattering. For this purpose, we use the expression for $\Sigma^<(p,q)$ and $\Gamma(p,q)$ given by Eqs. (55) and (56), respectively. The steady-state phonon Green's function can be more generally written as

$$D^<(\mathbf{k},E')=-i\gamma_k^2[(N_\mathbf{k}+1)B^e(\mathbf{k},E')+N_\mathbf{k}B^a(\mathbf{k},E')]\ , \tag{110}$$

$$D^>(\mathbf{k},E')=-i\gamma_k^2[(N_k+1)B^a(\mathbf{k},E')+N_\mathbf{k}B^e(\mathbf{k},E')]\ , \tag{111}$$

where $B^e(\mathbf{k},E')$ and $B^a(\mathbf{k},E')$ are the spectral weight functions for phonon emission and absorption, respectively, and $\gamma_\mathbf{k}^2$ represents the electron-phonon coupling. We define "emission profile function" $\eta^e_p(k)$ and "absorption profile function" $\eta^a_\mathbf{p}(k)$ as a convolution of electron and phonon spectral weight functions as follows:

$$\frac{1}{h^2}\int dE\,dE'A(\mathbf{p}+\mathbf{k},E+E',q)A(\mathbf{p},E,\mathbf{q})\gamma_\mathbf{k}^2B^e(\mathbf{k},E')$$
$$=\eta^e_\mathbf{p}(k)\ , \tag{112}$$

$$\frac{1}{h^2}\int dE\,dE'\,A(\mathbf{p}+\mathbf{k},E+E',\mathbf{q})A(\mathbf{p},E,\mathbf{q})\gamma_k^2 B^a(\mathbf{k},E') = \eta_p^a(\mathbf{k}) . \quad (113)$$

Note that in the absence of an electric field (intracollisional field effects) and any broadening of the electron and phonon spectral weight functions, $\eta_{\mathbf{p}}^e(\mathbf{k})$ and $\eta_{\mathbf{p}}^a(\mathbf{k})$ acquire very simple forms

$$\eta_{\mathbf{p}}^e(\mathbf{k}) = h\delta(E_{\mathbf{p}} - E_{p+k} + \Omega_k)\gamma_k^2 , \quad (114)$$

$$\eta_p^a(\mathbf{k}) = h\delta(E_p - E_{p+k} - \Omega_{\mathbf{k}})\gamma_k^2 , \quad (115)$$

which are simple statements of the energy-conservation law in an electron-phonon scattering process. In what follows, we may assume that the spectral-weight-function linewidth for phonons is independent of the field and wave vectors, hence it is a constant.

The alternate processes corresponding to Eqs. (114) and (115) are expressed through the relation

$$\eta_p^e(-\mathbf{k}) = \eta_{p-k}^a(\mathbf{k}) , \quad (116)$$

$$\eta_p^a(-\mathbf{k}) = \eta_{p-k}^e(\mathbf{k}) . \quad (117)$$

We write the results of Eqs. (98) and (99) as

$$-iG^<(\mathbf{p},E,\mathbf{q},t) = f_w(\mathbf{p}+e\mathbf{F}t)A(\mathbf{p},E,\mathbf{q}) , \quad (118)$$

$$iG^>(\mathbf{p},E,\mathbf{q},t) = [1-f_w(\mathbf{p}+e\mathbf{F}t)]A(\mathbf{p},E,\mathbf{q}) . \quad (119)$$

Applying the results of Eqs. (55) and (56) and (110)–(119), the expression for the collision terms, for a uniform scattering system in the presence of constant externally applied electric field, is given by

$$\begin{aligned}\frac{-i}{h}\int dE[\Sigma^<(p)A(p)-\Gamma(p)G^<(p)] = \sum_{\mathbf{k}}\{&\eta_p^e(\mathbf{k})(N_k+1)f_w(\mathbf{p}+\mathbf{k}+e\mathbf{F}t)[1-f_w(\mathbf{p}+e\mathbf{F}t)]\\ &+\eta_{\mathbf{p}-\mathbf{k}}^e(\mathbf{k})N_k f_w(\mathbf{p}-\mathbf{k}+e\mathbf{F}t)[1-f_w(\mathbf{p}+e\mathbf{F}t)]\\ &-\eta_p^e(\mathbf{k})N_k f_w(\mathbf{p}+e\mathbf{F}t)[1-f_w(\mathbf{p}+\mathbf{k}+e\mathbf{F}t)]\\ &-\eta_{p-k}^e(\mathbf{k})(N_k+1)f_w(\mathbf{p}+e\mathbf{F}t)[1-f_w(\mathbf{p}-\mathbf{k}+e\mathbf{F}t)]\} . \end{aligned} \quad (120)$$

In cases where the dependence on the energy variable E (or z) in the self-energies can be disregarded, we obtain the equation for the Wigner distribution function after integrating with respect to E,

$$\frac{\partial}{\partial t}f_w(\mathbf{p},\mathbf{q},t)+e\mathbf{F}\cdot\frac{\partial}{\partial\mathbf{p}}f_w(\mathbf{p},\mathbf{q},t) = \int\frac{-i}{h}dE[\Sigma^<(p,q)A(p,q)-\Gamma(p,q)G^<(p,q)] , \quad (121)$$

where the RHS is given by the RHS of Eq. (120), and $\eta_p^{e,a}(\mathbf{k})$ becomes

$$\eta_{\mathbf{p}}^{e,a}(\mathbf{k}) = 2\gamma_{\mathbf{k}}^2\mathrm{Re}\chi_p^{e,a}(\mathbf{k}) , \quad (122)$$

$$\begin{aligned}\chi_{\mathbf{p}}^{e,a}(\mathbf{k}) = \int_0^\infty d\tau\exp\Bigg[-\frac{1}{h}\int_0^\tau\Bigg\{&\Gamma\left[\mathbf{p}+\mathbf{k}+\frac{e\mathbf{F}\tau}{2}-e\mathbf{F}\tau'\right]+\tfrac{1}{2}\Gamma_{\mathrm{ph}}\\ &+i\Bigg[E_\alpha\left[\mathbf{p}+\mathbf{k}+\frac{e\mathbf{F}\tau}{2}-e\mathbf{F}\tau'\right]+\mathrm{Re}\Sigma^r\left[\mathbf{p}+\mathbf{k}+\frac{e\mathbf{F}\tau}{2}-e\mathbf{F}\tau'\right]\\ &-E_\alpha\left[\mathbf{p}+\frac{e\mathbf{F}\tau}{2}-e\mathbf{F}\tau'\right]-\mathrm{Re}\Sigma^r\left[\mathbf{p}+\frac{e\mathbf{F}\tau}{2}-e\mathbf{F}\tau'\right]\pm\Omega_k\Bigg]\Bigg\}d\tau'\Bigg] . \end{aligned} \quad (123)$$

The last equation represents an explicitly and fully gauge-invariant generalization of Lin and Chiu's result[28] for $\eta_{\mathbf{p}}^{e,a}(\mathbf{k})$, whereas results obtained from Eqs. (112) and (113) give the more rigorous expressions when dependence on the energy variable z cannot be neglected in a more general transport expression, Eq. (109).

VII. MORE REALISTIC CALCULATIONS TO INCLUDE FULL QUANTUM EFFECTS AND MANY-BODY SCATTERING FOR RTD's

The added value of the present formalism to quantum transport is that one can do numerical calculations which can account for quantum and/or many-body effects with the essentially invariant starting transport equation in a compact mathematical form. Section III demonstrates the inclusion of full quantum effects in real high-speed heterostructure devices. Section VI derives a nongradient-expansion quantum-transport equation for high electric fields, a problem that has received much attention in most quantum-transport calculations for submicron devices. In this section we will demonstrate that indeed calculations which account for full quantum effects and many-body scatterings can be done for RTD's in the relaxation-time approximation for the electron-phonon scattering, with remarkable results. Some results for electron-electron interaction in the spirit of the mean-field random-phase approximation have been accounted for by simultaneously solving the Poisson equation.[29] Depending on the advances that are made in calculating the self-energies, perhaps it is reasonable to hope that even more realistic calculations, with advance com-

putational resources, could be done in the future for the exact expression, Eq. (15).

In including scattering with the crystalline medium in this formulation, it would be desirable, for numerical convenience, to find the appropriate scattering operator C to append to the operator L in the RHS of Eq. (21) such that $ih\partial_t \mathbf{f}=(L+C)\mathbf{f}$. For simplicity, we assume that the effects of scattering on the quantum motion of the particle can be approximated by the zero-order gradient expansion of the collision term. In other words, the full quantum effects are treated to all orders in the gradient expansion as in Sec. III, but only the leading collision term is retained, which is identical to the collision term considered in the QBE. Further, as a first step in applying this formulation to RTD's, the collision term is numerically implemented using the relaxation-time approximation.

In this approximation we have to add to the RHS of Eq. (21) the QBE type of collision term which can be cast into the familiar "scattering out" and "scattering in" terms in a manner similar to the collision terms of the Boltzmann equation. A constant relaxation-time approximation, which is strictly valid near equilibrium and simplifies further the following demonstration, is obtained by writing down the collision terms added to the RHS of Eq. (21) of Sec. III as follows:

$$\sum_{\mathbf{p}} [W_{\mathbf{p}-\mathbf{p}'} f_w(\mathbf{p},\mathbf{q},t) - W_{\mathbf{p}'-\mathbf{p}} f_w(\mathbf{p},\mathbf{q},t)] = \frac{1}{\tau}\left[\frac{\rho(\mathbf{q},t)}{\rho_0(\mathbf{q})} f_0(\mathbf{p},\mathbf{q}) - f_w(\mathbf{p},\mathbf{q},t)\right], \quad (124)$$

where $f_0(\mathbf{p},\mathbf{q})$ is the Wigner function solution of RTD's in equilibrium or in the absence of any device terminal voltage bias, $\rho(\mathbf{q},t)=\sum_{\mathbf{p}} f_w(\mathbf{p},\mathbf{q},t)$ is the particle density, and τ is the constant relaxation-time calculated by considering all scattering mechanisms.

The choice of f_0 is constrained by requiring that $C\cdot\mathbf{f}_0=0$, which is the condition of "detailed balance" and that particle conservation is not violated. One choice, used by Frensley,[30] is to let $f_0=f_0(k)$, the thermal distribution of electrons in bulk GaAs, which then assures that the effects of the collision operator vanish in the boundaries. The choice we have made,[31] however, is to let $f_0=f_0(x,k)$, the unbiased steady-state distribution for the RTD; this choice is motivated by (a) the density of electrons and their distribution varies significantly in the presence of the barriers, and $f_0(x,k)$ addresses this, and (b) the condition of detailed balance is automatically satisfied in the simulation region for the unbiased case. Numerically, however, the difference in the calculated Wigner distribution function between the choices of $f_0(k)$ and $f_0(x,k)$ are small for the steady-state calculations, a reflection of the fact that the barrier region constitutes only a small portion of the simulation box size.

Obtaining appropriate or more realistic expressions for τ constitutes the next step.[31] To calculate an overall relaxation time, we have chosen to extract a relaxation time τ_i for each of the contributing processes (acoustic, zero-order optical, polar optical, piezoelectric, and ionized impurity scattering) by numerically integrating over the momentum relaxation time[31] according to

$$\tau_i = \int_0^{\infty} x^{3/2} e^{-x} \tau_m(x)/\Gamma(\tfrac{5}{2}) , \quad (125)$$

where Γ is the gamma function and $x=\beta E_k$, and combining the results according to Matthiessen's rule. Matthiessen's rule is known to be poor for electron densities around 1×10^{17} cm^{-3}, but for the parameters we are considering, the approximation is good. The numerical value of τ used for the calculations is then dependent only on temperature. The ionized impurity scattering is important at low temperatures, and only ionized and polar optical scattering is important at higher than room temperatures for the parameters we are considering.[31]

The presence of scattering mechanisms may be expected to interfere strongly with the resonant tunneling of electrons through the RTD at the resonant bias regions than for the high bias regions in which the tunneling is thought to be sequential or nonresonant. Our calculations confirm this trend: for a temperature range of $50\le T\le 300$ K, Fig. 7, the peak-to-valley current ratio is given by

$$I_p/I_v = R \ln(T_0/T) , \quad (126)$$

where $R=5.522$ and $T_0=451.4$ K, with an error of $\pm 3.9\%$. At higher temperatures, the ratio does not fall off as rapidly. Further, since scattering causes the electron distribution to approach $f_0(x,k)$, one may expect that the severe quantum oscillations in the Wigner function for biases near resonance will tend to be muted as the temperature increases (i.e., as τ decreases) and that the resonant trajectories[8] will become degraded and appear more sequential. This is in fact the case. For calculations at resonance, the severity of the oscillations in the Wigner function [Figs. (8) and (9)] decreases as the temperature increases; $\partial_x f$ at the boundaries becomes smaller as well, which has the added advantage of making the assumed boundary conditions more accurate for the troublesome resonant regions. Note that for $T=300$ K

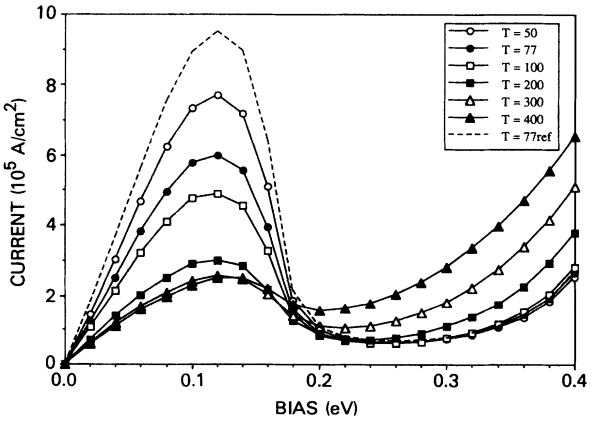

FIG. 7. The I-V characteristic of the RTD at different temperatures. All scattering mechanisms are taken into account within the relaxation-time approximation.

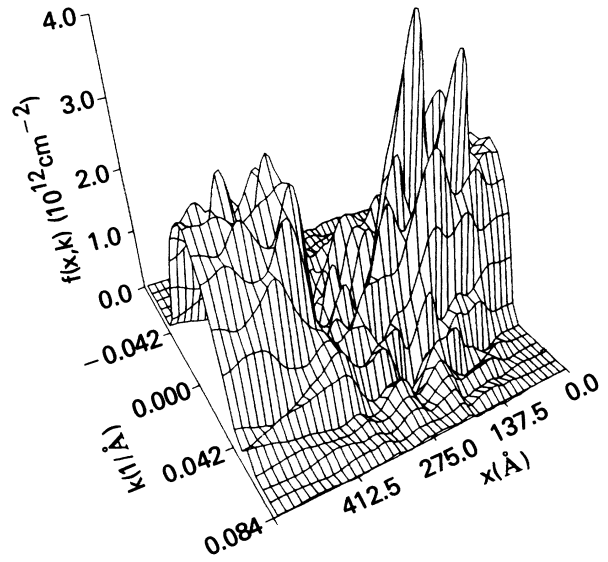

FIG. 8. Wigner distribution function solution for the RTD at 77 K and biased at resonance ($V_0=0.116$ eV, $\tau=525.2$ fs). This figure is to be compared with Fig. 9 plotted at 300 K.

($\tau=97$ fs), the peaks in the Wigner function are greatly suppressed by comparison to $T=77$ K ($\tau=525$ fs). The tunneling ridge, which is discernible at 77 K, is almost completely eliminated at $T=300$ K, Fig. 10. Calculations for small bias[31] have shown that the trajectories (which, for the steady-state case, correspond to the contour lines[10]) almost reduce to the unbiased case as T exceeds room temperature, Fig. 11(b), whereas for low temperatures, the resonant trajectories, though affected, retain some degree of the resonant-tunneling characteristics, as can be seen in Fig. 11(a).

As collisions between electrons and phonons would tend to dampen the flow of electrons, one might expect that a collision term will suppress the oscillations present

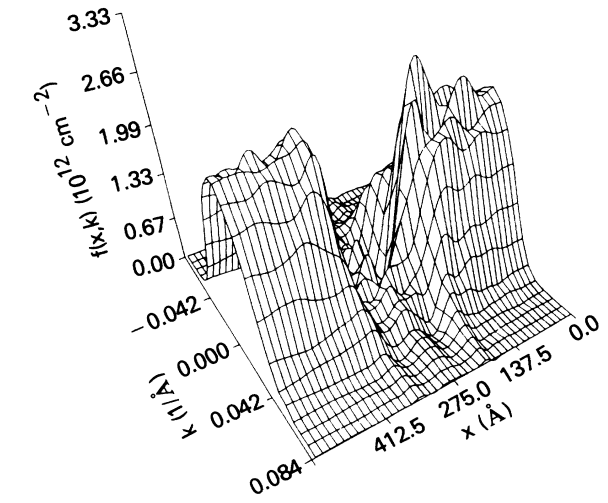

FIG. 9. Wigner distribution function solution for the RTD at 300 K and biased at resonance ($V_0=0.116$ eV, $\tau=97.4$ fs).

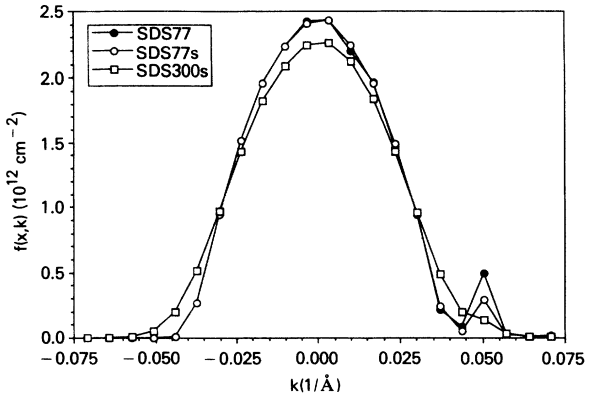

FIG. 10. Comparison of the quantum distribution function at the drain end of the RTD, plotted at different temperatures corresponding to Figs. 8 and 9. The solid circles are values at 77 K without scattering, plotted for comparison. Observe that the tunneling ridge is almost eliminated at room temperature.

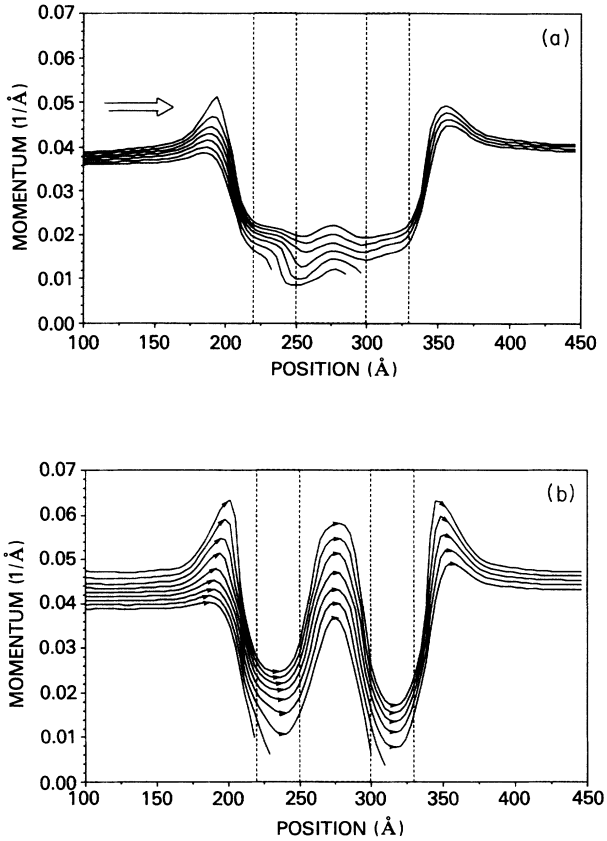

FIG. 11. (a) The Wigner trajectory pattern corresponding to Fig. 4(b), when scattering corresponding to 77 K ($\tau=525.2$ ft) is switched on in the simulation. Broken paths are trajectories that turned back and failed to tunnel through. (b) The Wigner trajectory pattern corresponding to (a), when the temperature is raised to 300 K. The resulting tunneling pattern resembles the trajectory pattern of Fig. 3(b) for the RTD at zero bias which is referred to here as "sequential tunneling." Broken trajectories are paths that turned back and failed to tunnel through.

in the time evolution of the current density $J(x)$ which appears to be due to electrons collecting in and tunneling out and bouncing back and forth against the wall of the quantum well, while the electron density adjusts to the new bias. We have run simulations at $T=77$ K and 300 K to find how the transient current response is affected [Figs. 12(a) and 12(b)]. It is apparent that the oscillations are diminished greatly by comparison to the collisionless case, and that in the room-temperature case the oscillations are almost completely destroyed. Consequently, the addition of a collision term has the paradoxical effect of decreasing the switching time of a RTD since it essential-

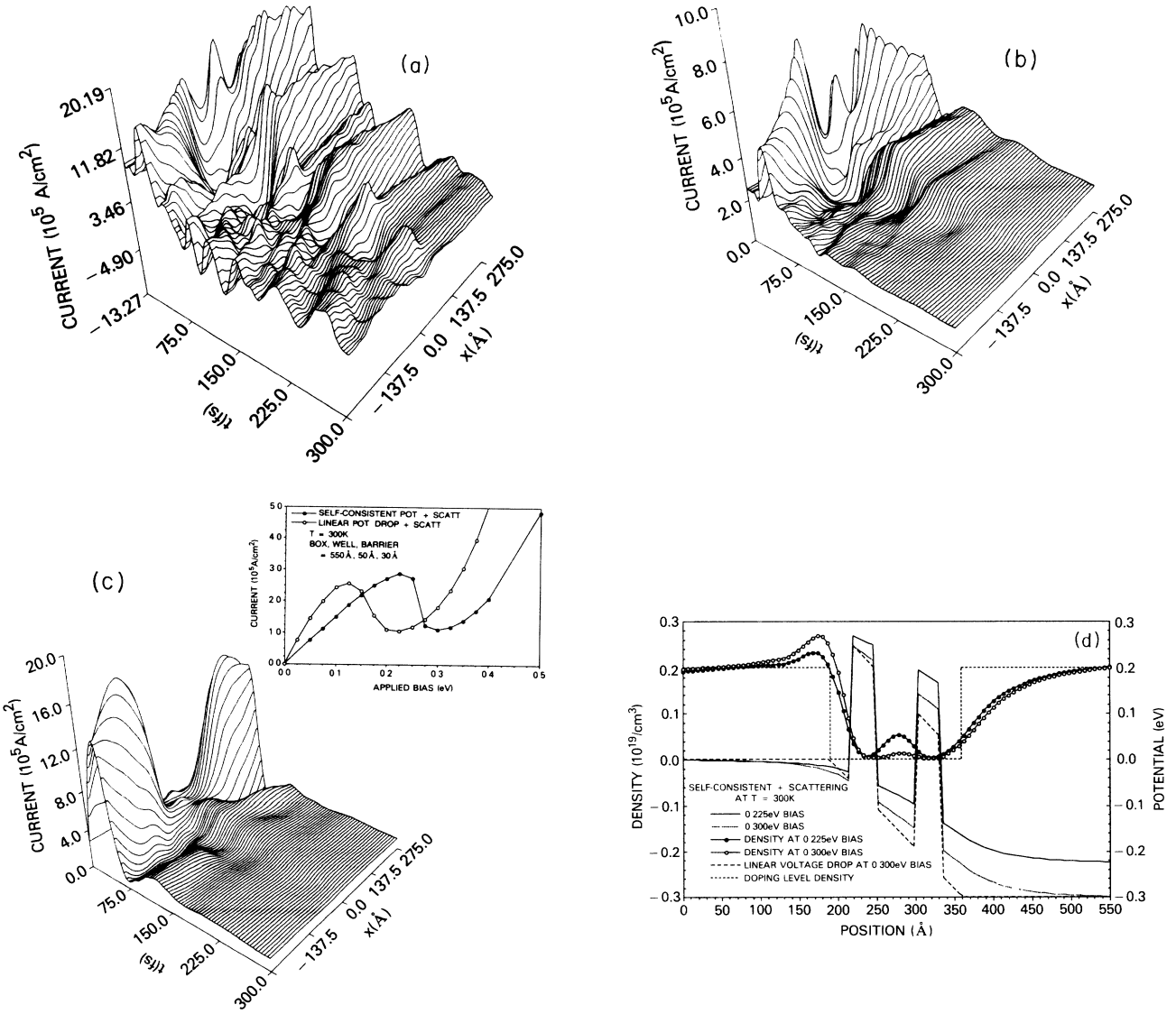

FIG. 12. (a) Transient response of the current-density distribution to a sudden switch in the voltage bias as in Fig. 6(c), when scattering corresponding to 77 K ($\tau=525.2$ fs) is switched on in the simulation. (b) Transient response of the current-density distribution to a sudden switch in the voltage bias corresponding to (a), when the temperature is raised to 300 K ($\tau=97.4$ fs). Observe the shorter switching time compared to (a). (c) Transient response of the current-density distribution to a sudden switch in the voltage bias, including the effect of the self-consistent potential, at 300 K corresponding to (b). The effect of the self-consistent potential and charge distribution (i.e., electron-electron interaction in the mean-field random-phase approximation) have been included by simultaneously solving the Poisson equation, at each time step, in a transient simulation. The self-consistent potential and charge simulations, including the steady-state conditions, were all performed using the transient simulator. The resonant current-peak and valley-minimum biases have shifted to higher values in the self-consistent calculations as compared to those of Fig. 7, obtained for a simple linear voltage drop across the device. In (c), switching was performed from the current-peak value of 0.225 eV to the current-valley-minimum value of 0.30 eV. (d) Self-consistent potential and electron density distribution corresponding to the end states of (c). The self-consistent potential for the bias of 0.30 eV is shown compared with the linear voltage drop, an approximation used in all the other simulations. Depending on the computational box size, a "drifted" Fermi distribution with drift velocity equal to the product of the low-field mobility and the electric field at the boundary may be employed as a self-consistent boundary condition for the incoming electrons. Doping density of 2.0×10^{18} cm^{-3} extends from the source and drain of the RTD up to 30 Å before the barrier edges.

ly eliminates the long-term quantum oscillations if the temperature is large enough.

In summary, the effect of the inclusion of a simple relaxation-time collision operator is in accordance with expectations in its effects on the steady-state characteristics of I-V curves and particle trajectories since (a) the peak values and peak-to-valley ratio of the I-V curves decrease as the relaxation time decreases, (b) the resonant particle trajectories become more sequential in appearance, and (c) the oscillations and tunneling ridges are muted by comparison to the collisionless case. For temperatures less than 76 K, the mean free path of the electrons is greater than 170 Å, the length over which the bias is applied in the simulated RTD. In the case of switching times, a collision operator has the unusual effect of decreasing the switching time, primarily by decreasing the long time tail behavior of the current transient response. Finally, Fig. 12(c) shows the affect of including electron-electron interactions by solving the Poisson equation for self-consistent space charge and potential to account for electron-electron interactions in a mean-field random-phase approximation.[29]

The effect of self-consistency on the I-V characteristics is similar to the experimentally known effect of a resistor connected in series with an Esaki tunnel diode, as shown in the inset of Fig. 12(c). New features in the negative differential resistance (NDR) portion of the I-V curve were also observed in our simulations, particularly at 77 K, in agreement with the experimental results for GaAs/AlGaAs RTD's. Indeed, the NDR region in our simulation exhibits high-frequency ($\sim$2.5 THz) oscillating currents (approximately sinusoidal) in contrast to the region outside of the NDR. This is the first time to our knowledge that this has been seen in a computer simulation. By taking the time-average current values at each bias point in this region, the resultant I-V exhibits the characteristic "plateaulike" structure, in agreement with the experiments. These NDR features in our simulations, including the simulated intrinsic dynamical bistability of the current and/or space charge, and comparison with the experiments will be discussed in more detail in a separate paper.

Although the treatment of many-body effects given here is not totally self-consistent (the collision operator is only zeroth order in the gradient expansion), the physically appealing quality of the results clearly demonstrates the power and usefulness of the quantum distribution approach to the realistic simulation of quantum-based devices. To date, no other quantum approach has been fruitfully used in characterizing high-speed quantum-based active devices. Recently, Frensley[30] has employed a similar approximation to the collision term to investigate the effects of collisions on the I-V device characteristics of RTD's. This paper serves to clarify his approximation which was guided by making an analogy to the Boltzmann equation. Since $f_w(\mathbf{p},\mathbf{q})$ is a strong function of $\mathbf{q}$ in RTD even at steady state[8,10] and, furthermore, since $f_w(\mathbf{p},\mathbf{q})$ is far from thermal equilibrium where complete detailed balance holds, this approximation is not self-consistent. The "Fokker-Planck collision operator" in $\mathbf{k}$ space also employed by Frensley[30] does not seem to have any theoretical basis within the many-body quantum-transport theory since all derivatives are governed by the Poisson bracket operator. Moreover, all the above approximations are clearly suspect for transient simulations of RTD's. Serious numerical work is urgently needed for more accurate treatment of scatterings and collisions in quantum transport.

VIII. CONCLUSIONS

We have presented a well-rounded and exact formalism of the quantum-distribution-function approach in many-body quantum-transport theory, for systems (in general, highly transient and nonuniform in space) whose dynamics depend on the direction of time in three- and four-dimensional vector "phase space." The formalism is expected to pave the way for the present Wigner distribution-function approach to evolve towards a more accurate technique for the simulation of quantum-based high-speed devices, and allows one to formally judge the accuracy of various approximation schemes. The formalism serves to unify various approaches based on (a) the generalized quantum Boltzmann equation, (b) the time-evolution equation of the Wigner distribution function (first derived by Wigner), (c) density-matrix projection operator techniques, and (d) path-integral techniques[20] through the nonequilibrium Green's-function formalism. Indeed, some efforts have also been directed towards other potentially accurate methods, e.g., the use of real-time path-integral techniques.[32] It has not yet demonstrated its applicability towards a realistic and transient simulation of nanometric quantum-based devices, in contrast to the use of the quantum-distribution-function approach.[8-10]

While it may be true that the "nonlocal" nonequilibrium Green's-function formalism alone (i.e., infinite space and time), without subsidiary device boundary conditions, cannot describe an active open system, it is the principal assumption of this paper that the addition of a self-consistent subsidiary device boundary condition, which describes the particle exchanges and interactions with the outside environment, for a finite (hence "open") system fully describes the state of that finite open system as time evolves according to the quantum distribution transport equation formulated in this paper. In effect, and this is true for both classical and quantum treatment (in general to integro-differential equations in mathematical physics), the boundary condition "integrates out" the degrees of freedom outside the device region of interest. At present, we cannot furnish a rigorous proof for this; the validity of this assumption rests solely on a "correspondence principle," in the self-consistency of the numerical results, and on agreement with the experimental data for RTD's. Indeed, in the limit $\hbar \to 0$, a typical device problem, including the subsidiary device boundary condition, exactly reproduces the problem of a classical finite active open system described by the Boltzmann equation. The exact corresponding classical problem, which typically makes an assumption of the distribution of incoming particle distribution, is routinely used in particle Monte Carlo semiconductor device simulations[33]

and in plasma physics device numerical simulations,[34] where electrical contact to the device is modeled by an unchanging large number of charge carriers (neutralized by the background charges) at zero electric field and consequently incoming electrons from the contact are usually assumed to be thermally distributed, corresponding to the classical limit of the "$k_\perp$-integrated" Fermi-Dirac equilibrium distribution function used in this paper. The same assumptions are often used for charge carriers coming from a highly screened, heavily doped region (far from the active regions) of the device, and their self-consistency verified in the numerical simulation. All these assumptions imply the presence of sufficiently relaxing and irreversible processes (Markovian) in the regions outside the device.[8]

Further, since in general the nonequilibrium Green's-function formalism merely describes the evolution of a time-irreversible system starting from a noncorrelated state[35] at, say, $t = -\infty$, steady state is not defined for all times. Again we rely on the correspondence principle and in the numerical self-consistency of the results, using the quantum-distribution-function approach developed here, in assuming that the application of the voltage bias, together with the subsidiary boundary condition, allows the system to evolve to a steady state after some finite time t_0 of interest. Steady-state conditions for the exact corresponding classical problems ($\hbar \to 0$) using the Boltzmann equation is again a routine result in classical transport modeling. The physically meaningful and self-consistent numerical results and fair agreement of the quantum calculations with experimental data on RTD also serve to further validate the assumptions made in this paper in applying the formalism to real high-speed devices.

The power of the lattice Weyl-Wigner formalism of quantum transport presented here not only lies in the simplicity and compactness of the exact results but more importantly in its ability to simulate open boundary conditions existing in real devices, very much like the use of the classical Boltzmann equation, and the ensuing well-behaved numerical stability inherent in the simple mathematical form possessed by the exact integro-differential quantum-transport equation. The authors would like to draw the readers attention to the computer simulation results for the RTD whose drain voltage is suddenly switched from the peak-current voltage value to the valley-current voltage value, Figs. 6(a), 6(b), 12(a), 12(b), and 12(c). These are clear and physically meaningful demonstrations of how active RTD's respond to the sudden change of voltage at the drain. These figures enable one to read off the value of inherent device switching times, a figure of merit. What is worth pointing out is that the current response contains in general a wide band of frequencies in the Fourier transform to the frequency domain. These signify the difficulty which the quantum-transport approach, based on the use of wave functions, has to face, i.e., one needs a very large number of basis states, aside from the need to be able to describe violent mixing of these basis states, to describe quantum coherence and interference caused by the sudden change of voltage bias. The statistical nature, and by virtue of the fact that it has exact classical correspondence including the subsidiary device boundary conditions, renders the distribution-function approach more advantageous than the wave-function or density-matrix approach. Furthermore, the quantum-distribution-function approach enables us to easily define quantum particle trajectories, to better understand quantum-transport processes, and to allow the coupling of a quantum-transport technique with the powerful ensemble particle Monte Carlo technique.

An elegant treatment of Bloch electrons in the presence of an externally applied uniform electromagnetic field follows the lattice Weyl-Wigner quantum-mechanical techniques employed by one of the authors (F.A.B.) in previous works,[13,14] as demonstrated in Sec. VI, since the formalism used here goes far beyond[13,36] the continuum level of quantum dynamics. The results given here are applicable to more accurate numerical simulations of emerging high-speed heterostructure quantum-based electronic devices. The "tight-binding" or crystal-lattice formulation[13,14] can, in principle, account for the complicated and "renormalized band structure" and scattering energetics of the whole heterostructure device, and offers first-principle treatment of heterostructure "intervalley" dynamics and effective-mass variations. The exact numerical solution of Eq. (15), together with Eq. (8), would involve standard iterative techniques, including self-consistency checks for ensuring conservation laws (Ward-Takahashi identities[37]) for various approximation to the Green's function, characteristic of all many-body calculations. Equation (15) is easier to numerically implement than corresponding path-integral approaches;[32] it includes full quantum effects, unlike previous many-body quantum-transport studies,[4–7] and is therefore expected to impact on the advances of the numerical simulation of quantum-based devices of great technological importance.

Finally, it should be remarked that a limited view was adopted in previous applications of the Wigner distribution-function equation to open systems,[8] which was rooted in the apparent realization that this equation is derivable from the Schrödinger equation with Hermitian or "time-reversible" Hamiltonians. Therefore there was some conceptual difficulty in trying to apply the Wigner distribution-function equation to irreversible open systems and various means of justification have been put forward.[8] The formalism given here is free from this difficulty since the conceptual base of nonequilibrium quantum transport is founded specifically for systems whose dynamics are dependent on the direction of time, as was first discussed by Schwinger.[3] Application of the exact quantum-transport equation to open systems therefore has similar implications and corresponding consequences as the ubiquitous applications of the Boltzmann equation to classical open systems, by invoking the correspondence principle discussed above.

ACKNOWLEDGMENTS

The authors are grateful to the Office of Naval Research and the Office of Naval Technology for the support of this work.

APPENDIX A: NONEQUILIBRIUM GREEN'S-FUNCTION FORMALISM

For a nonequilibrium or nonstationary irreversible system, where the dynamics is dependent on the direction of time, no state of the system in the future may be identified with any state in the past. For this reason, expectation values and Green's functions are defined on a contour, in which the time arguments runs from the initial time t_0 to the "far" future (e.g., largest time argument of the Green's function) and then back to t_0. With this definition, a perturbation expansion of the Green's function along the path is analogous to the conventional many-body equilibrium Green's-function expansion and a separation of many-body interaction terms into self-energy parts and single-particle Green's-function terms is justified for expectation values defined along this contour.

With time arguments along the contour, the nonequilibrium Green's function is defined as

$$iG(x_1,t_1,x_2,t_2)\equiv\langle T[\hat{\Psi}_H(x_1,t_1)\hat{\Psi}_H^{\dagger}(x_2,t_2)]\rangle , \tag{A1}$$

where the time-ordering operator T orders the time argument along the contour. Thus we may write

$$G(x_1,t_1,x_2,t_2)=\Theta(t_1,t_2)G^{>}(x_1,t_1,x_2,t_2) +\Theta(t_2,t_1)G^{<}(x_1,t_1,x_2,t_2) , \tag{A2}$$

where $\Theta(t_1,t_2)=1$ if t_1 is later on a contour than t_2, and $\Theta(t_1,t_2)=0$ if t_1 is earlier than t_2. Employing Feynman's perturbation expansion method or Schwinger's variational[38] method for introducing the self-energy, the Green's function satisfies integral equations with time arguments defined on the contour in the usual fashion as

$$\oint d2\, G^{-1}_{\alpha\sigma}(1,2)G_{\sigma\beta}(2,1')=\delta_{\alpha\beta}(1,1') , \tag{A3}$$

$$\oint d2\, G_{\alpha\sigma}(1,2)G^{-1}_{\sigma\beta}(2,1')=\delta_{\alpha\beta}(1,1') . \tag{A4}$$

Separating the "self-energy," we have the equations of motion obeyed by the Green's function

$$\left[-\frac{\hbar}{i}\frac{\partial}{\partial t_1}-E_\alpha\left[-\frac{\hbar}{i}\nabla_1\right]\right]G_{\alpha\beta}(1,1') =\delta_{\alpha\beta}(1,1')+\oint \Sigma_{\alpha\sigma}(1,2)G_{\sigma\beta}(2,1') \tag{A5}$$

$$\left[\frac{\hbar}{i}\frac{\partial}{\partial t_{1'}}-E_\alpha\left[\frac{\hbar}{i}\nabla_{1'}\right]\right]G_{\alpha\beta}(1,1') =\delta_{\alpha\beta}(1,1')+\oint d2\, G_{\alpha\sigma}(1,2)\Sigma_{\sigma\beta}(2,1') . \tag{A6}$$

The "self-energy" Σ has the following general form:[34,38]

$$\Sigma_{\alpha\beta}(1,2)=\delta(t_1,t_2)\Sigma^{\rm VHF}_{\alpha\beta}(\mathbf{q}_1,\mathbf{q}_2,t_1)+\Theta(t_1,t_2)\Sigma^{>}_{\alpha\beta}(1,2) +\Theta(t_2,t_1)\Sigma^{<}_{\alpha\beta}(1,2) , \tag{A7}$$

where

$$\Sigma^{\rm VHF}=V(\mathbf{q}_1)\delta_{\alpha\beta}(1,1')+\Sigma^{\rm HF}_{\alpha\beta}(\mathbf{q},\mathbf{q}_1',t_1) , \tag{A8}$$

and $V(\mathbf{q}_1)$ is the external potential and $\Sigma^{\rm HF}_{\alpha\beta}(\mathbf{q},\mathbf{q}_1,t_1)$ is the Hartree-Fock approximation to the self-energy. In the above equations, $E_\alpha(\mathbf{k})$ is the exact energy-band function for band index α, time integration is along the contour, and the Einstein summation convention for the greek indices is used. Dropping the greek indices (one-band model) and using the definition of retarded and advanced functions in real-time axis, we write Eqs. (A5) and (A6) in a representation-independent form as follows:

$$-\frac{\hbar}{i}\frac{\partial}{\partial t_1}G^{\gtrless}(1,1')=\mathcal{H}G^{\gtrless}+\Sigma^{r}G^{\gtrless}+\Sigma^{\gtrless}G^{a} , \tag{A9}$$

$$\frac{\hbar}{i}\frac{\partial}{\partial t_{1'}}G^{\gtrless}(1,1')=G^{\gtrless}\mathcal{H}+G^{r}\Sigma^{\gtrless}+G^{\gtrless}\Sigma^{a} , \tag{A10}$$

where

$$\mathcal{H}(1,2)=\left[E_\alpha\left[-\frac{\hbar}{i}\nabla_1\right]+V(1)\right]\delta(1-2) +\delta(t_1-t_2)\Sigma^{\rm HF}(x_1,x_2,t_1) . \tag{A11}$$

The inclusion of the exchange term introduces nonlocality in space in the effective potential included in $\mathcal{H}$. Subtracting Eq. (A10) from Eq. (A9) leads to Eq. (1) given in the text, which is the same as that obtained by the analytic continuation procedure.[39] The Dyson equations corresponding to Eqs. (A5) and (A6) are

$$G_{\alpha\beta}(1,1')=G^0_{\alpha\beta}(1,1')+\oint d2\oint d3\, G^0_{\alpha\sigma}(1,2)\Sigma_{\sigma\eta}(2,3) \times G_{\eta\beta}(3,1') , \tag{A12}$$

$$G_{\alpha\beta}(1,1')=G^0_{\alpha\beta}(1,1')+\oint d2\oint d3 G_{\alpha\sigma}(1,2)\Sigma_{\sigma\eta}(2,3) \times G^0_{\eta\beta}(3,1') . \tag{A13}$$

Converting Eq. (A12) to real-time axis integration according to Schwinger,[3] Craig,[18] and Keldysh[2] and employing the linear canonical matrix transformation of Keldysh,[2] the following matrix equation results (here $F=G^{>}+G^{<}$):

$$\begin{bmatrix}0 & G^a\\ G^r & F\end{bmatrix}=\begin{bmatrix}0 & G^{0a}\\ G^{0r} & F^0\end{bmatrix}+\begin{bmatrix}0 & G^{0a}\Sigma^aG^a\\ G^{0r}\Sigma^rG^r & F^0\Sigma^aG^a+G^{0r}(\Omega G^a+\Sigma^rF)\end{bmatrix} . \tag{A14}$$

Equation (A14) yields the integral equation for G^r, G^a, and F,

$$G^r=G^{0r}+G^{0r}\Sigma^rG^r , \tag{A15}$$

$$G^a=G^{0a}+G^{0a}\Sigma^aG^a , \tag{A16}$$

$$F=F^0(1+\Sigma^aG^a)+G^{0r}(\Omega G^a+\Sigma^rF) . \tag{A17}$$

Equations (A15)–(A17) can be used to derive an integral expression from $G^{\gtrless}$. The same result for the integral form of $G^{\gtrless}$ can be obtained directly from Eq. (A12) by converting the integration to real-time axis, and by employing Schwinger's definition of the matrix form of the nonequilibrium Green's function in real-time axis[3] but without the use of the Keldysh transformation[2] to yield the following matrix relation:

$$\begin{bmatrix} G^c & -G^< \\ -G^> & \tilde{G}^c \end{bmatrix} = \begin{bmatrix} G_0^c & -G_0^< \\ -G_0^> & \tilde{G}_0^c \end{bmatrix} + \begin{bmatrix} \begin{bmatrix} G_0^c(\Sigma^c G^c - \Sigma^< G^>) \\ -G_0^<(\Sigma^> G^c - \tilde{\Sigma}^c G^>) \end{bmatrix} & \begin{bmatrix} G_0^c(\Sigma^< \tilde{G}^c - \Sigma^c G^<) \\ -G_0^<(\tilde{\Sigma}^c \tilde{G}^c - \Sigma^> G^<) \end{bmatrix} \\ \begin{bmatrix} G_0^>(\Sigma^c G^c - \Sigma^< G^>) \\ -\tilde{G}_0^c(\Sigma^> G^c - \tilde{\Sigma}^c G^>) \end{bmatrix} & \begin{bmatrix} G_0^>(\Sigma^< \tilde{G}^c - \Sigma^c G^<) \\ -\tilde{G}_0^c(\tilde{\Sigma}^c \tilde{G}^c - \Sigma^> G^<) \end{bmatrix} \end{bmatrix}, \tag{A18}$$

where $G^c(=G^r+G^<)$ stands for the chronological Green's function and $\tilde{G}^c[=-(G^a-G^<)]$ is the antichronological Green's function with similar definition for the self-energies. Equating the matrix elements for $G^{\gtrless}$ we have

$$G^{\gtrless}=G_0^{\gtrless}(1+\Sigma^a G^a)+G_0^r(\Sigma^{\gtrless}G^a+\Sigma^r G^{\gtrless}) , \tag{A19}$$

which can also be written as

$$G^{\gtrless}=G^r\Sigma^{\gtrless}G^a+(1+G^r\Sigma^r)G_0^{\gtrless}(1+\Sigma^a G^a) . \tag{A20}$$

The differential time-evolution equation for $G^{r,a}$ and F can similarly be easily obtained by converting Eqs. (A5) to real-time axis, according to Schwingers,[3] Craig,[17] Korenmann,[15] or Keldysh.[2] The resulting expression for $G^{r,a}$ is given in Sec. VI.

APPENDIX B: EXACT INTEGRAL OPERATOR OF THE QUANTUM-TRANSPORT EQUATION

Let us denote the Weyl transform of two operators $\hat{A}$ and $\hat{B}$ as $a(p,q)$ and $b(p,q)$, respectively. The Weyl transform of $\hat{A}\hat{B}=\hat{C}$ is denoted as $c(p,q)$. Then we have the following relation:

$$c(p,q)=e^{i\hat{\Lambda}}a(p,q)b(p,q) , \tag{B1}$$

where $\hat{\Lambda}$ is the Poisson-bracket operator used in the text. First let us evaluate the following expression:

$$\exp\left[-i\frac{\hbar}{2}\frac{\partial^{(a)}}{\partial p}\cdot\frac{\partial^{(b)}}{\partial q}\right]a(p,q)b(p,q) .$$

We do this by first writing the Weyl transform $a(p,q)$ and $b(p,q)$ as Fourier-transformed quantities

$$a(p,q)=\int dv\, e^{(i/\hbar)p\cdot v}K^a(q-\tfrac{1}{2}v,q+\tfrac{1}{2}v) , \tag{B2}$$

$$b(p,q)=\int du e^{(i/\hbar)q\cdot u}K^b(p+\tfrac{1}{2}u,p-\tfrac{1}{2}u) . \tag{B3}$$

Making use of well-known "exponential" displacement operation, we thus obtain

$$\exp\left[-i\frac{\hbar}{2}\frac{\partial^{(a)}}{\partial p}\cdot\frac{\partial^{(b)}}{\partial q}\right]a(p,q)b(p,q) = \frac{1}{h^4}\int du\, dq' e^{(i/\hbar)(q-q')\cdot u}a\left[p+\frac{u}{2},q\right]b(p,q') , \tag{B4}$$

where the inverse Fourier-transform relations corresponding to Eqs. (B2) and (B3) were used to bring back Weyl transformed quantities in Eq. (B4).

Let us write $b(p,q')$ in Eq. (B4) by making use of the alternate expression of Eq. (B3) as

$$b(p,q')=\int dv\, e^{(i/\hbar)p\cdot v}K^b(q'-\tfrac{1}{2}v,q'+\tfrac{1}{2}v) . \tag{B5}$$

Applying the remaining differential operation in the Poisson bracket occurring in the exponent $\hat{\Lambda}$, proceeding in a similar manner as before, and noting that the sum and difference of $a(p+j,q-v/2)$ and $a(p-j,q+v/2)$ is "even" and "odd", respectively, in the variables j and v, we finally arrived at the following expressions:

$$\sin(\hat{\Lambda})a(p,q)b(p,q)=\frac{1}{(h^4)^2}\int dq'dp'\left\{\int dv\, dj\left[a\left[p+j,q-\frac{v}{2}\right]-a\left[p-j,q+\frac{v}{2}\right]\right]\times\sin\left[\frac{2j}{\hbar}\cdot(q'-q)\right]i\sin\left[\frac{(p'-p)}{\hbar}\cdot v\right]\right\}b(p',q') , \tag{B6}$$

$$\cos(\hat{\Lambda})a(p,q)b(p,q)=\frac{1}{(h^4)^2}\int dq'dp'\left\{\int dv\, dj\left[a\left[p+j,q-\frac{v}{2}\right]+a\left[p-j,q+\frac{v}{2}\right]\right]\times\cos\left[\frac{2j\cdot(q'-q)}{\hbar}\right]\cos\left[\frac{p'-p}{\hbar}\cdot v\right]\right\}b(p',q') . \tag{B7}$$

We have chosen to write the kernel of the integral operator in Eqs. (B6) and (B7) in the form given by Eqs. (16) and (17) in the text since in the absence of scattering and collision the integral over j can often be carried out when written in the form given in the text.

APPENDIX C: THE KADANOFF-BAYM ANSATZ

Recently Lipavsky, Spicka, and Velicky[26] (LSV) proposed a generalized Kadanoff-Baym (KB) ansatz by writing $G^{\gtrless}$ as a product of two operators, one being the density-matrix operator for electrons or holes. The idea is to separate the operator whose Weyl transform gives the Wigner distribution function for electrons or holes. However, we see in Appendix B that in general, granted that the separation can be done, the resulting Weyl transform of $G^{\gtrless}$ will not be a simple product of the Weyl transform of the particle density-matrix operator and that of the Weyl transform of the other operator (obtained by some *ad hoc* choice by LSV). The question then becomes, what is a more accurate way of achieving the separation so that the Weyl transform is approximated by simple product of Weyl transforms?

As originally proposed by LSV, the generalized KB ansatz is written, in our notation, as

$$-iG^{\gtrless}=i(G^{r}\rho^{\gtrless}-\rho^{\gtrless}G^{a}) , \tag{C1}$$

where the Weyl transform[13] of $p^{<}$ (electron density-matrix operator) is the Wigner distribution function. We can immediately see that the Weyl transform of $-iG^{<}$ is equal to $A(p,q)f_{w}(p,q)$ plus first-order and higher-order gradient corrections.

A more accurate ansatz can easily be obtained by writing Eq. (C1) as

$$-iG^{\gtrless}=\frac{i}{2}\{G^{r},\rho^{\gtrless}\}-\frac{i}{2}\{\rho^{\gtrless},G^{a}\} \tag{C2}$$

which is clearly equal to $A(p,q)\rho^{\gtrless}(p,q)$ plus second-order and higher-gradient corrections. Equation (C2) is the generalized KB ansatz referred to in the text; it is more accurate and retains the full symmetry between electrons and holes.

[1] L. P. Kadanoff and G. Baym, *Quantum Statistical Mechanics* (Benjamin, New York, 1962).

[2] L. V. Keldysh, Zh. Eksp. Teor. Phys. **47**, 1515 (1964) [Sov. Phys.—JETP **20**, 1018 (1965)].

[3] J. Schwinger, J. Math. Phys. **2**, 407 (1961).

[4] A. P. Jauho and J. W. Wilkins, Phys. Rev. B **29**, 1919 (1984).

[5] A. P. Jauho, Phys. Rev. B **32**, 2248 (1985).

[6] F. S. Kahn, J. H. Davies, and J. W. Wilkins, Phys. Rev. B **36**, 2578 (1987).

[7] G. D. Mahan, Phys. Rep. **145**, 251 (1987).

[8] W. Frensley, Phys. Rev. B **36**, 1570 (1987). Earlier work in using the Wigner distribution function to tunneling problems was attempted by J. R. Barker, D. W. Lowe, and S. Murray, in *The Physics of Submicron Structures,* edited by H. L. Grubin, K. Hess, G. J. Iafrate, and D. K. Ferry (Plenum, New York, 1984), p. 277.

[9] K. L. Jensen and F. A. Buot, J. Appl. Phys. **65**, 5248 (1989).

[10] K. L. Jensen and F. A. Buot, Appl. Phys. Lett. **55**, 669 (1989).

[11] U. Ravaioli, M. A. Osman, W. Potz, N. Kluksdahl, and D. K. Ferry, Physica B **134**, 36 (1987).

[12] F. A. Buot and K. L. Jensen (unpublished).

[13] F. A. Buot, Phys. Rev. A **33**, 2544 (1986).

[14] F. A. Buot, Phys. Rev. B **14**, 3310 (1976); **14**, 977 (1976); **10**, 3700 (1974); Phys. Rev. A **8**, 1570 (1973); **9**, 211 (1974).

[15] V. Korenman, Ann. Phys. (N.Y.) **39**, 72 (1966).

[16] K. L. Jensen and F. A. Buot, J. Appl. Phys. **67**, 2153 (1990).

[17] C. Dewdney and B. J. Hiley, Found. Phys. **12**, 27 (1982). See also B. J. Hiley, in *Bell's Theorem, Quantum Theory and Conceptions of the Universe,* edited by M. Kafatos (Kluwer, Dordrecht, 1989), pp. 181–190.

[18] R. A. Craig, and J. Math. Phys. **9**, 605 (1968).

[19] However, see Ref. 35, and V. Korenman, J. Math. Phys. **10**, 1387 (1969), for exceptional cases.

[20] J. W. Negele and H. Orland, *Quantum Many-Particle Systems* (Addison-Wesley, New York, 1988).

[21] R. D. Mattuck, *A Guide to Feynman Diagrams in Many-Body Problem* (McGraw-Hill, New York, 1976).

[22] R. J. Elliott, J. A. Krumhansl, and P. L. Leath, Rev. Mod. Phys. **46**, 465 (1974).

[23] J. C. Inkson, *Many-Body Theory of Solids* (Plenum, New York, 1984).

[24] J. M. Ziman, Electrons and Phonons (Clarendon, Oxford, 1960).

[25] H. Haken, *Quantum Field Theory of Solids* (North-Holland, Amsterdam, 1976).

[26] P. Lipavský, V. Špička, and B. Velický, Phys. Rev. B **34**, 6933 (1986).

[27] G. H. Wannier, Rev. Mod. Phys. **34**, 645 (1962).

[28] J. Lin and L. C. Chiu, J. Appl. Phys. **57**, 1373 (1985); Appl. Phys. Lett. **54**, 919 (1988).

[29] F. A. Buot, Phys. Rev. B **14**, 977 (1976).

[30] W. Frensley, Solid State Electron. **31**, 739 (1988). See also N. C. Kluksdahl, A. M. Kriman, C. Ringhoper, and D. K. Ferry, *ibid.* **31**, 743 (1988).

[31] K. J. Jensen and F. A. Buot, J. Appl. Phys. **67**, 7602 (1990).

[32] B. A. Mason and Karl Hess, Phys. Rev. A **39**, 5051 (1989).

[33] C. Moglestue, IEEE Trans. Comput. Aided Design **CAD-5**, 326 (1986); Comput. Methods Appl. Mech. Eng. **30**, 173–208 (1982); see also F. A. Buot, Compel **6**, 45 (1987).

[34] J. M. Dawson, Rev. Mod. Phys. **55**, 403 (1983).

[35]P. Danielewicz, Ann. Phys. (N.Y.) **152**, 239 (1984).
[36]F. A. Buot, in *Bell's Theorem, Quantum Theory and Conceptions of the Universe*, edited by M. Kafatos (Kluwer, Dordrecht, 1989), pp. 159–162.
[37]M. Revsen, T. Toyoda, Y. Takahashi, and F. C. Khanna, Phys. Rev. B **40**, 769 (1989).
[38]T. Kato, T. Kobayashi, and M. Namiki, Prog. Theor. Phys. Suppl. **15**, 3 (1960).
[39]D. C. Langreth and J. W. Wilkins, Phys. Rev. B **6**, 3189 (1972).